TARCO GROUP

Thompson Ramo Wooldridge Inc.

Cleveland 17, Ohio

DISCLAIMER

MND-P-2379
ENGINEERING REPORT 4054

SNAP I POWER CONVERSION SYSTEM BEARINGS DEVELOPMENT

PREPARED BY

NEW DEVICES LABORATORIES, TAPCO GROUP
THOMPSON RAMO WOOLDRIDGE INC.

AS AUTHORIZED BY

THE MARTIN CO. PURCHASE ORDER OE 0101

FOR

THE UNITED STATES ATOMIC ENERGY COMMISSION
PRIME CONTRACT AT(30-3)-217

1 FEBRUARY 1957 TO 30 JUNE 1959

PUBLISHED 20 JUNE 1960

PREPARED BY:

R. Meredith
G. Y. Ono
D. C. Reemsnyder

LEGAL NOTICE

This report was prepared as an account of Government sponsored work. Neither the United States, nor the Commission, nor any person acting on behalf of the Commission:

A. Makes any warranty or representation, expressed or implied, with respect to the accuracy, completeness, or usefulness of the information contained in this report, or that the use of any information, apparatus, method, or process disclosed in this report may not infringe privately owned rights; or

B. Assumes any liabilities with respect to the use of, or for damages resulting from the use of any information, apparatus, method, or process disclosed in this report.

As used in the above, "person acting on behalf of the Commission" includes any employee or contractor of the Commission to the extent that such employee or contractor prepares, handles or distributes, or provides access to, any information pursuant to his employment or contract with the Commission.

DISTRIBUTION LIST

		Copy No.
1.	Commander, AFBMD Hq., USAF ARDL P.O. Box 262 Inglewood, California For: Maj. G. Austin	1
2.	Commander, ARDC Andrews Air Force Base Washington 25, D. C. Attn: RDTAPS, Capt. W. G. Alexander	2
3.	Army Ballistic Missile Agency Commanding General Army Ballistic Missile Agency Redstone Arsenal, Alabama Attn: ORDAB-c	3, 4
4.	U. S. Atomic Energy Commission Technical Reports Library Washington 25, D. C. Attn: Mr. J. M. O'Leary For: Lt. Col. G. M. Anderson, DRD Capt. John P. Wittry, DRD Lt. Col. Robert D. Cross, DRD R. G. Oehl, DRD Edward F. Miller, PROD Technical Reports Library	5 through 10
5.	Atomics International Division of North American Aviation, Inc. P. O. Box 309, Canoga Park, California Attn: Dr. Chauncey Starr For: J. Wetch	11
6.	Chief, Bureau of Aeronautics Washington 25, D. C. Attn: C. L. Gerhardt, NP	12

DISTRIBUTION LIST (Continued)

		Copy No.
7.	Chief, Bureau of Ordnance Dept. of the Navy, 4110 Main Navy Bldg. Washington 25, D. C. Attn: Mrs. R. Schmidt or G. Myers To be opened by addressee only for: Ren, SP	13, 14
8.	Chief, Bureau of Ships Department of the Navy, Code 1500 Washington 25, D. C. Attn: Melvin L. Ball	15
9.	U. S. Atomic Energy Commission Canoga Park Area Office P. O. Box 591 Canoga Park, California Attn: A. P. Pollman, Area Manager	16
10.	U. S. Atomic Energy Commission Chicago Operations Office P. O. Box 59, Lemont, Ill. Attn: A. I. Mulyck For T. A. Nemzek, Mr. Klein	17, 18
11.	Office of the Chief of Naval Operations Department of the Navy Washington 25, D. C.	19
12.	Atomic Division Office of Chief of Research & Development Department of the Army Washington 25, D. C.	20
13.	Commanding Officer Diamond Ordnance Fuse Laboratories Washington 25, D. C. Attn: ORDTL 06.33, Mrs. M. A. Hawkins	21 through 23

DISTRIBUTION LIST (Continued)

		Copy No.
14.	U. S. Atomic Energy Commission Hanford Operations Office P. O. Box 550 Richland, Washington Attn: Technical Information Library	24
15.	Lockheed Aircraft Corporation Missile Systems Division Palo Alto, California Attn: Mr. Hal H. Greenfield	25, 26
16.	Monsanto Chemical Company Mound Laboratory P. O. Box 32, Miamisburg, Ohio Attn: Library and Records Center For: Mr. Roberson	27
17.	National Aeronautics & Space Administration Ames Aeronautical Laboratory Moffett Field, California Attn: Smith J. de France, Director	28
18.	National Aeronautics & Space Administration Langley Aeronautical Laboratory Langley Field, Virginia Attn: Henry J. E. Reid, Director	29
19.	National Aeronautics & Space Administration Lewis Flight Propulsion Laboratory 21000 Brookpark Road Cleveland 35, Ohio Attn: George Mandel	30
20.	Commander U. S. Naval Ordnance Laboratory White Oak, Silver Spring, Maryland Attn: Eva Lieberman, Librarian	31 through 33

DISTRIBUTION LIST (Continued)

		Copy No.
21.	Director Naval Research Laboratory, Code 1572 Washington 25, D. C. Attn: Mrs. Katherine H. Cass	34
22.	U. S. Atomic Energy Commission New York Operations Office 376 Hudson Street New York 14, New York Attn: Reports Librarian	35, 84
23.	Union Carbide Nuclear Company X-10, Laboratory Records Department P. O. Box X Oak Ridge, Tennessee Attn: Eugene Lamb	36
24.	Office of Naval Research Department of the Navy, Code 735 Washington 25, D. C. Attn: E. E. Sullivan For: Code 429	37
25.	Director, USAF Project Rand Via AF Liaison Of., The Rand Corporation 1700 Main St., Santa Monica, California Attn: F. R. Collbohm For: Dr. J. Huth	38
26.	Commander, Rome Air Development Center Griffiss Air Force Base, New York Attn: RCSG, J. L. Briggs	39
27.	U. S. Atomic Energy Commission Reference Branch Technical Information Service Extension Oak Ridge, Tennessee	40 through 64

DISTRIBUTION LIST (Continued)

		Copy No.
28.	Thompson Ramo Wooldridge Staff Research and Development New Devices Laboratories P. O. Box 1610, Cleveland 4, Ohio	65, 66, 67
29.	Univ. of Calif. Radiation Lab Technical Information Division P. O. Box 808, Livermore, Calif. Attn: C. G. Craig For: Dr. H. Gordon	68
30.	Commander, Wright Air Dev. Center Wright-Patterson Air Force Base, Ohio Attn: WCACT For: Capt. N. Munson, WCLPS, G. W. Sherman, WCLEE, WCOSI	69 through 72
31.	Commanding Officer Jet Propulsion Laboratory Pasadena, California Attn: W. H. Pickering, I. E. Newlan	73
32.	Univ. of California Radiation Lab Technical Information Division P. O. Box 808, Livermore, California Attn: Clovis G. Craig For: Dr. Robert H. Fox	74
33.	Los Alamos Scientific Laboratory P. O. Box 1663 Los Alamos, New Mexico Attn: Report Librarian For: Dr. George M. Grover	75
34.	Commander Air Force Special Weapons Center Technical Information & Intelligence Office Kirtland Air Force Base, New Mexico Attn: Kathleen P. Nolan	76

DISTRIBUTION LIST (Continued)

		Copy No.
35.	School of Aviation Medicine Brooks Air Force Base, Texas	77
36.	Commander Aero-space Technical Intelligence Center Wright-Patterson Air Force Base, Ohio Attn: H. Holzbauer, AFCIN-4 Bla	78
37.	National Aeronautics & Space Administration 1512 H. Street, N. W., Washington 25, D. C. Attn: Dr. Addison M. Rothrock	79 through 83
38.	The Martin Company P. O. Box 5042, Baltimore 20, Maryland Attn: AEC Document Custodian	86 through 90
39.	Advanced Research Project Agency The Pentagon, 3D154, Washington 25, D. C. Attn: Fred A. Koether or Donald E. Percy	85

FOREWORD

SNAP I is the first of a family of devices to convert nuclear energy to electrical for use in space. The SNAP Systems for Nuclear Auxiliary Power - programs are sponsored by the Atomic Energy Commission; the SNAP I prime contractor is The Martin Company. SNAP I was designed to utilize a radio isotope as the energy source.

The SNAP I Power Conversion System utilizes mercury as the working fluid for a Rankine cycle. A radioisotope is used as the energy source to vaporize mercury in a boiler; turbo-machinery extracts the useful energy from the vapor and converts it into electrical energy; the exhaust vapor is condensed by rejecting the waste thermal energy to space in a condenser-radiator.

During the SNAP I Power Conversion System development, Thompson Ramo Wooldridge has been responsible for the development of the following items:

Turbo-machinery

- Mercury vapor turbine
- Alternator
- Lubricant and condensate pump
- Mercury lubricated bearings

Speed Control

Condenser-Radiator

A series of eight Engineering Reports have been prepared describing Thompson Ramo Wooldridge's SNAP I Power Conversion System development program. These are as follows:

ER-4050	Systems
ER-4051	Turbine
ER-4052	Alternator
ER-4053	Pump
ER-4054	Bearings
ER-4055	Control
ER-4056	Condenser-Radiator
ER-4057	Materials

The material in this report deals specifically with the developmental history of the bearings for the SNAP I Power Conversion System. This report is submitted as part of the requirements of Purchase Order OE-0101 from the Martin Company, issued under the Atomic Energy Commission prime contract AT(30-3)-217.

TABLE OF CONTENTS

1.0 SUMMARY

The SNAP I bearing development program consisted of the analysis, design, fabrication and testing of several types of hydrosphere bearings. Preliminary analysis and experimental testing indicated that a hydrosphere bearing, which is a mated spherical journal and hemispherical socket, would best satisfy the SNAP I requirements. Primary design considerations were reliability, low power loss, sufficient load capacity, and minimum lubricant flow requirements. The hydrosphere bearing offers combined thrust and radial load capacity, good dynamic stability, misalignment capability, close control of clearances for other rotating components, and utilization of the working fluid as a lubricant. Two 1/2 inch diameter hydrospheres with flow restrictions in the sockets were selected for the final SNAP I bearings.

Analytical and empirical hydrosphere bearing design procedures were evolved and verified by experimental results. Experimental results also verified that the hydrosphere bearing performance was within design specifications.

Two test rigs were designed, fabricated and used for development testing of liquid mercury lubricated bearings.

The final hydrosphere bearing was successfully incorporated in pump-bearing subsystem tests and final system integration and tests. The SNAP I power conversion system exceeded its original 60 day life specification in a system endurance test. The system accumulated 2510 hours of endurance testing. It was shut down on schedule without defect and provided a conclusive demonstration of mercury lubricated bearing endurance capabilities.

2.0 INTRODUCTION

Figure 2-1 shows the turbo-machinery package of SNAP I--the first space powerplant. This unique subminiature electric power generator contains the turbine, alternator, and condensate pump for the Rankine cycle power conversion system. These components are mounted on a common shaft rotating at 40,000 rpm and supported by mercury lubricated bearings.

Required to operate unattended for long durations in stringent environments, the SNAP I turbo-machinery package is the result of advanced engineering concepts in analysis, design, fabrication, and experimentation.

This report describes the efforts that culminated in the bearings for this package.

To meet the requirements imposed on the SNAP I turbo-machinery, preliminary investigations resulted in the selection of liquid mercury lubricated hydrosphere bearings. The object of this report is to review the reasons for selection; trace the background and development history of the bearings; present the theoretical design of the bearing; compare it with experimental results; and to summarize the actual performance of the hydrosphere bearings.

The particular hydrosphere configuration with which this report is primarily concerned consists of a ball journal mating with a slightly larger diameter socket incorporating an integral flow restriction.

Flow, frictional power loss, and axial and radial load capacities are the performance parameters which are discussed in this report. Performance of the basic bearing, the bearing-flow restriction subassembly and pairs of bearing assemblies are evaluated. Life and startup requirements and bearing materials selection are reviewed.

SNAP I TURBOMACHINERY PACKAGE

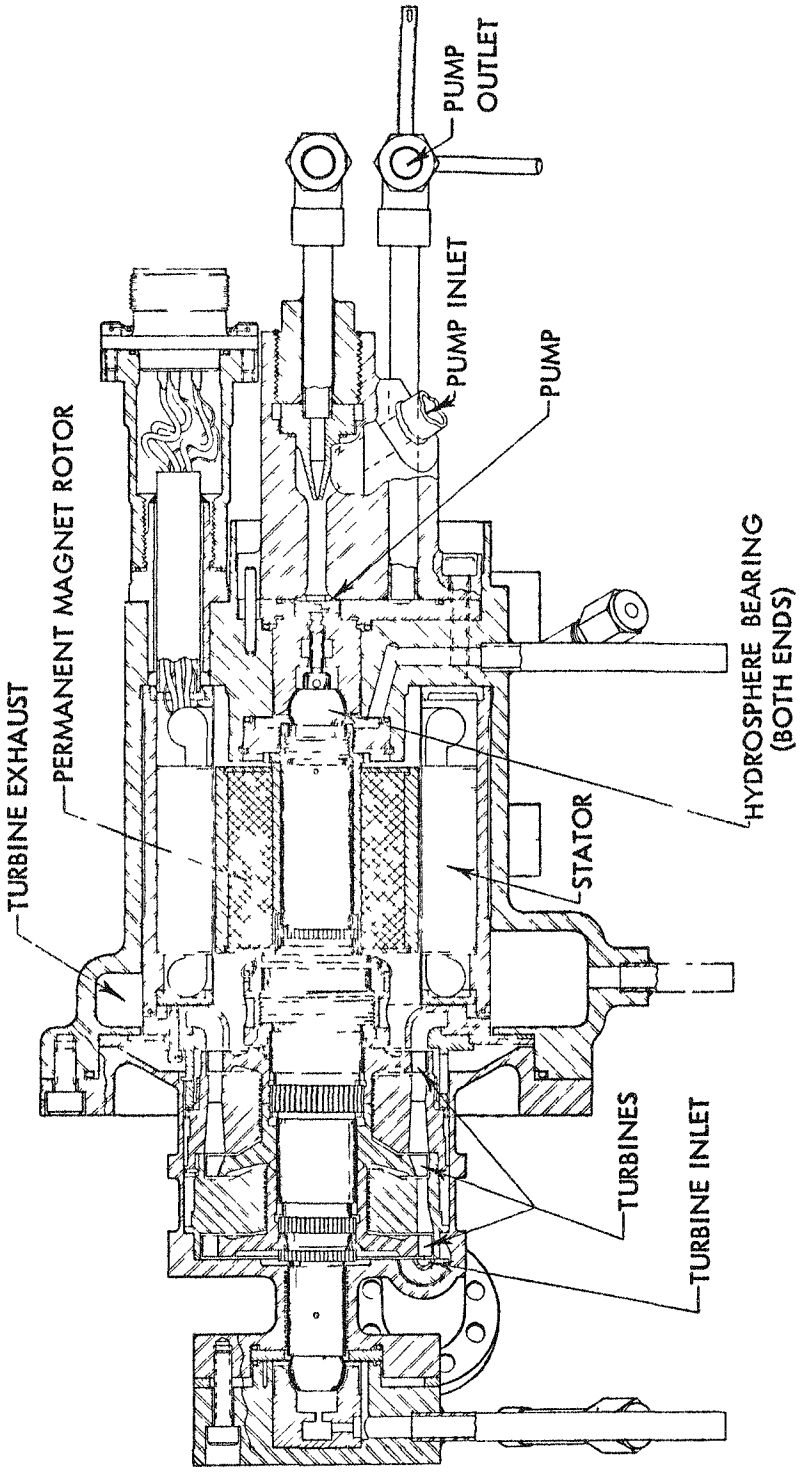

FIGURE 2-1

3.0 BEARING REQUIREMENTS AND SELECTION

Rankine Space Power Conversion Systems require turbo-machinery bearings which allow long, consistent, reliable action. The bearings chosen must provide a minimum parasitic torque when exposed to any of the following loads:

1. Axial and radial loads imposed by the shaft mounted equipment.
2. Loads due to thermal and loading deformations.
3. Acceleration loads.
4. Vibration loads.
5. Gyroscopic loads.

In addition to supporting the above loads, the bearings must also provide:

1. Accurate positioning of the shaft and turbine seals.
2. Small variation in fluid leakage from the cold start to the stable running conditions.
3. A seal for the working fluid or utilize it as the lubricating fluid.
4. Sufficient allowance for reasonable amounts of lubricant contamination.
5. For changes in angular velocity and load.

Using the above requirements and considerations plus overall system requirements the design objectives formulated for the bearings are shown in Table 3-1.

Five bearing types were investigated as possible for this application. A general description of each type follows.

1. Liquid lubricated hydrodynamic journal and thrust bearings were not considered certain to be dynamically stable for the high speeds and light loads for this specific application. Bearing instability could be manifested in dry whirl, film vibration, layer instability and film cavitation. The operational conditions also necessitated the use of two pairs of journal thrust bearing combinations and the resultant high power loss could not be tolerated.

2. Gas or vapor lubricated hydrodynamic bearings were considered to have the possibility of similar instability characteristics. The excessive quantity of flow required to insure thick film lubrication was also intolerable.

3. Anti-friction bearings did not have adequate assurance of life or reliability. Thermal stability and materials compatibility of the conventional bearing materials presented problems. Power and life requirements precluded the use of seals, and hence, of secondary lubricants, and the use of mercury as a lubricant for rolling contact elements did not appear desirable.

TABLE 3-1

DESIGN OBJECTIVES

Speed	40,000 rpm
Lubricant	Liquid Mercury
Power Absorption (2 bearings)	400 watts
Flow (2 bearings)	10 lbs/min
Lubricant supply temperature	350°F
Lubricant supply pressure	250 psia
Life	60 days (1440 hours)
Load capacity	20 lbs thrust
	20 lbs radial
	3 lbs bearing unbalance
Acceleration	8g in any direction
Eccentricity	.0025 inch, radial
Unpressurized start under 1g load	
Dynamically stable	

4. Pressurized hydrostatic journal and thrust bearings had possibilities of similar instability characteristics and required more bearings, as did their hydrodynamic counterparts. In addition, the alighment precision and high flows required by hydrostatic bearings appeared infeasible.

5. The hydrosphere, shown in Figure 3-1 and Figure 3-2, is a mated spherical journal and hemispherical socket. Its application as a bearing is known to date back to 1887. Although its application since then has been limited, certain observed advantages made it of especial interest for the application under consideration.

   Film vibration, layer instability, turbulence and other phenomena causing shaft whirl at speeds between the critical and one-half critical have been found to be a function of bearing clearance. When the film approaches boundary layer thickness, the most stable conditions exist. Because of the difficulty in measuring flow in small passages, the conclusions drawn are based on the results of various design modifications rather than exact identification of conditions within the bearing passages. Others have found experimentally that oil film whirl occurs at lower speeds as the clearance of a full journal bearing increases. Because of this it was suspected that the hydrosphere should be stable at high speed. Inspection of the bearing cross section, shown in Figure 3-1, reveals small equatorial clearances and that axial movement of the shaft does not induce proportional changes in this radial clearance. Previous investigators, who undertook the study of the hydrosphere as a hydrodynamic bearing, and those who have developed a high speed conical bearing, have expressed the opinion that small clearances are required.

   Since the heat generated by fluid shear must be absorbed in the flowing fluid, a minimum flow rate must be set for each specific bearing. Pumping power also limits the practical upper value of flow rate. The hydrosphere was found to fit these limits.

   The fact that the hydrosphere is insensitive to misalignment is a distinct advantage since bearing loadings due to warpage from residual housing strains and unequal thermal distribution should be avoided. The more conventional journal and thrust face is alignment sensitive, but the hydrosphere does not require that the axis of rotation of the sphere be coincident with the geometric axis of the socket.

   The hydrosphere has both an axial and a radial load carrying capacity due to pressure distribution. An additional radial load carrying capacity arises from viscous centering forces.

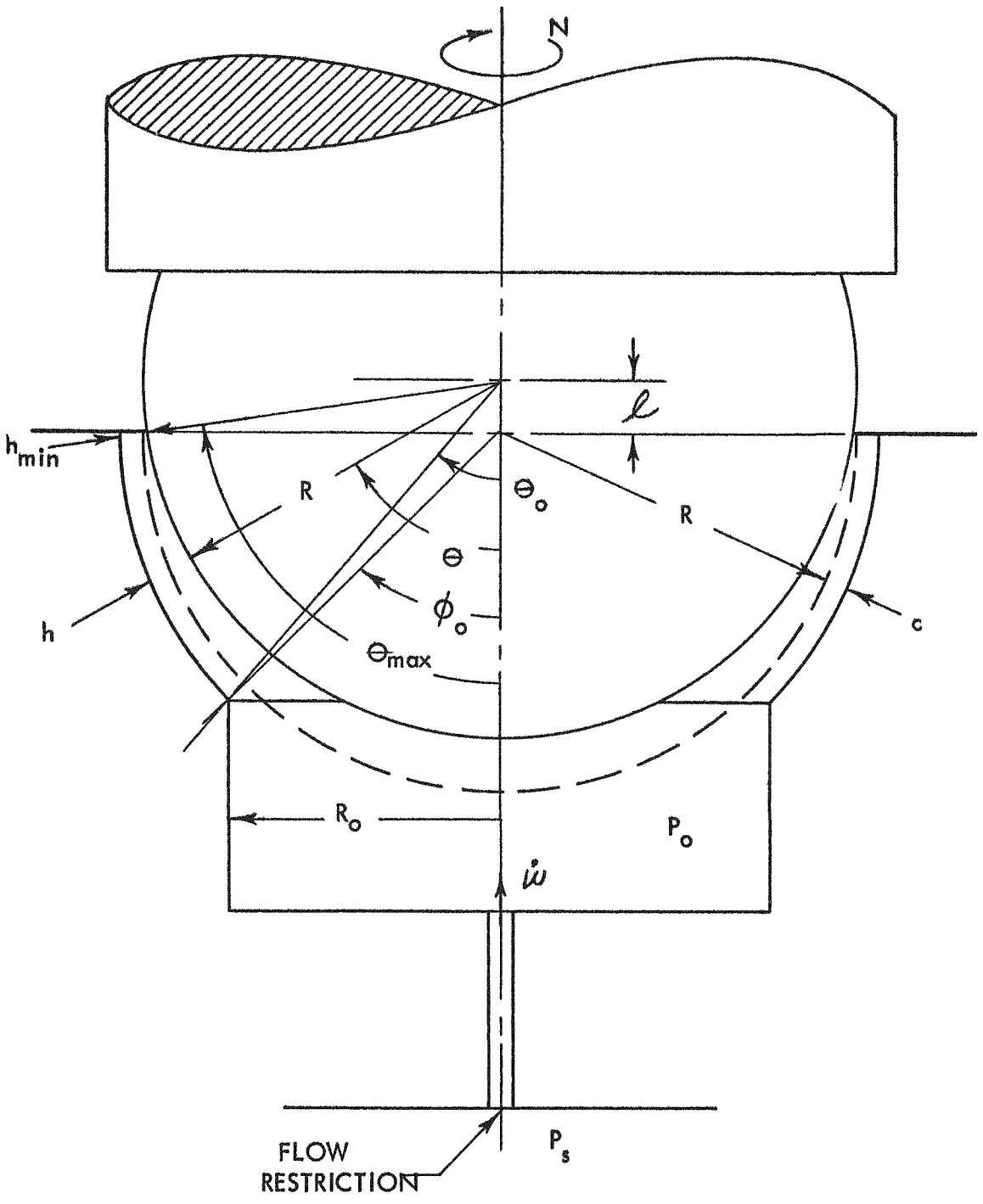

HYDROSPHERE BEARING ASSEMBLY

FIGURE 3-1

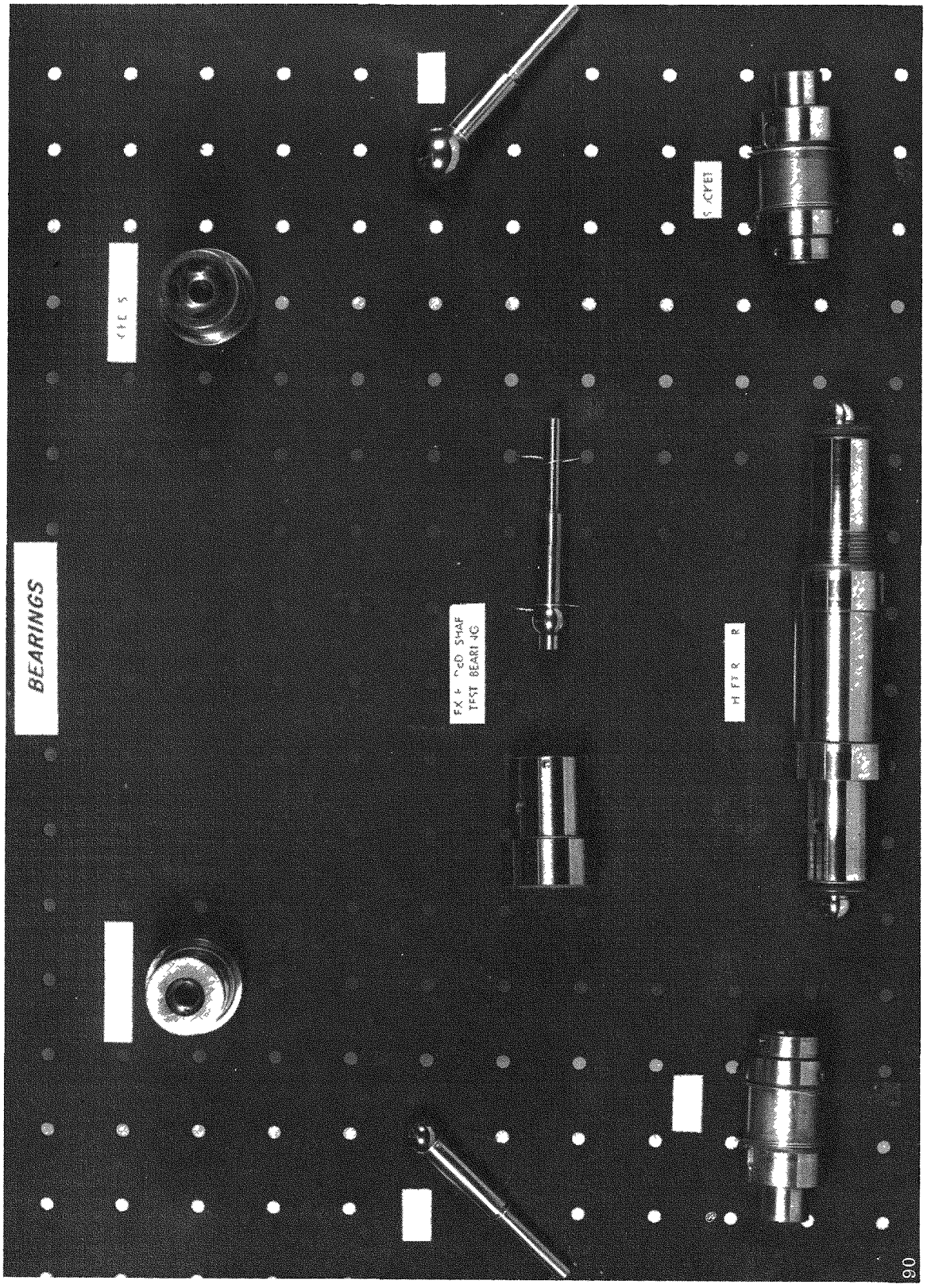

HYDROSPHERE BEARING HARDWARE

FIGURE 3-2

A disadvantage of the hydrosphere was its precision fabrication requirements. In addition, like most pressurized hydrostatic bearings, unless there is some device to increase bearing pressure with increasing axial load the bearing will collapse, shutting off lubricant flow and result in bearing seizure. Such a device may be a restricting orifice in the bearing inlet line. The system then is essentially a dual orifice system with flow being a function of lift, and a properly designed orifice in the inlet line will cause the bearing pressure to increase as the bearing sphere approaches the socket, thereby compensating for the load increase. This type of control may take the shape of an orifice, a capillary tube, or a porous filter. The hydrosphere depends on maintaining relatively small equatorial clearance changes over a large temperature range. This can be controlled by using similar materials for the ball and socket.

In summary, the hydrosphere bearing is attractive because of combined thrust and radial load capacity, good dynamic stability, misalignment capability, close control of clearances for other rotating components, ease of utilization of the working fluid as a lubricant, and low power consumption. These advantages resulted in its selection as the bearings for SNAP 1.

Selection of the type of lubricant presented a problem due to the requirement that the power conversion system working fluid must be kept free of foreign matter such as bearing oils. Three solutions to the problem were considered:

1. Incorporate a high temperature, high speed rotating positive seal to keep the lubricant separated from the cycle fluid. Static seals are also necessary to keep the bearing lubricant out of the package during shipping and storage.

2. The use of dry rolling contact type bearings.

3. The utilization of the system fluid, i.e., mercury, as a lubricant.

Conventional type lubricants were eliminated from consideration due to the following resultant problems:

1. The state of the art for seals was such that positive sealing could not be insured for the 60 days required life of the package.

2. The high temperature, especially at the turbine end, plus the nuclear radiation was too severe an environment for conventional lubricants.

3. The bearing lubricant would require an additional pump which would decrease the reliability of the system.

Dry rolling contact type bearings would also require seals to prohibit entry of wear particles into the system working fluid or mercury into the bearings.

Therefore, it was concluded that the most logical solution was to develop a high temperature liquid mercury lubricated bearing.

4.0 HYDROSPHERE BEARING DEVELOPMENT

4.1 Background

Early work on the hydrosphere bearing was done by M. C. Shaw and C. D. Strang with conventional lubricants (1) (2)*. Their attempts of mathematical analysis resulted in a solution which was not completely practical due to its complexity and its utilization of parameters which could not be determined experimentally. Consequently most of their work was of an empirical nature. Also, most of Shaw and Strang's reported tests were made with axially loaded bearings, although some mention was made of radial load tests.

Preliminary analyses and tests of the hydrosphere bearings were started at the New Devices Laboratories of Thompson Ramo Wooldridge in 1956. On the basis of these analyses and tests with liquid mercury as the lubricant, and after consultation with a number of experts in this field, hydrosphere bearings were finally selected as the most promising type for small power mercury engine application.

Initial development of these bearings involved sockets having grooves in the axial plane and mating perfectly with the spherical journal. Radial load tests showed the grooves to limit capacity to values less than the SNAP I requirements. For these and other reasons, the hydrosphere bearing in its current state of development is a "loosely" fitting ball mated with a nongrooved socket as shown in Figure 3-1. The total bearing assembly includes a flow restriction to control socket pressure.

4.2 Theoretical Approach

An approach to the analytical solution of hydrosphere bearings, but not the solution itself, was presented by Shaw and Strang (1) and (2). As can be seen from Figure 3-1 the lubricant film is crescent-shaped in any plane through the axis of rotation, if the ball center is axially displaced outward from the socket center. Since this wedge shape is not in the direction of motion and since the density and viscosity of the fluid are assumed constant throughout the film, the manner in which hydrodynamic pressures are developed to support axial loads is not immediately apparent. Shaw and Strang proposed that the pressure is developed along a mean streamline as shown in Figure 4-1. This streamline is a helix starting at the inlet hole (or groove, depending on socket configuration) and ends at the equator. By definition, the net flow across the vertical walls of the stream tube is zero. Using this somewhat unconventional approach, they arrived at the following relationship:

$$\frac{\partial}{\partial S}\left(\frac{\rho}{12N}\, l^{3} \cos^{3}\theta\, \frac{\partial P}{\partial S}\, dn\right) = \frac{l\, Rw}{4}\, \frac{\partial}{\partial S}\left(\rho \sin 2\theta \sin \alpha\, dn\right)$$

*Letters in parentheses refer to the Bibliography listed at the conclusion of this report.

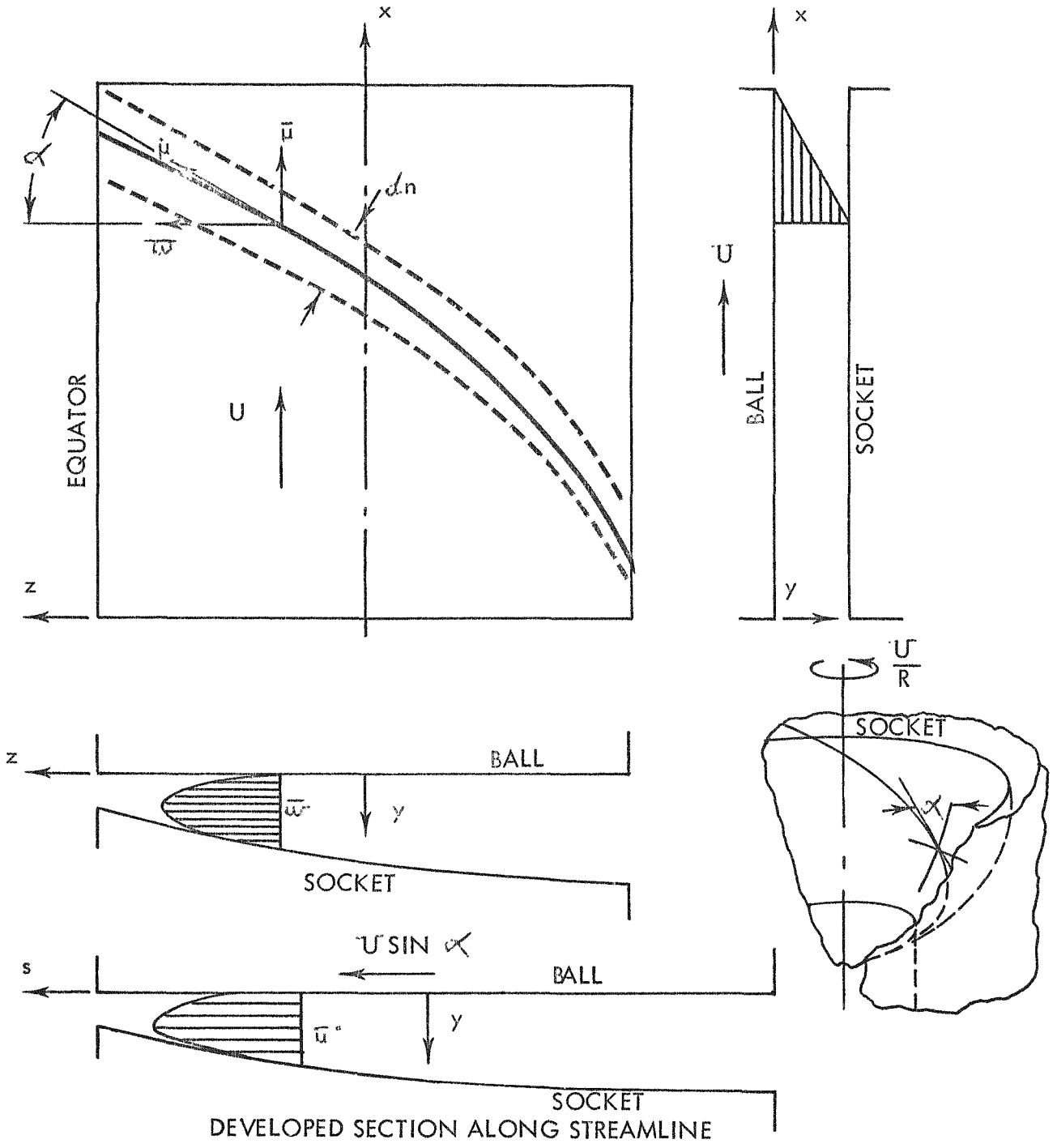

SHAW AND STRANG'S MEAN STREAM TUBE FOR THE UNWRAPPED HYDROSPHERE BEARING

FIGURE 4-1

Because the manner in which P , α and dn vary with S could not be analytically determined, the equation was left unsolved and the remainder of the report was restricted to a discussion of test results.

4.3 Experimental Development

Based on the preliminary theoretical analysis of different bearing types the hydrosphere bearings received first priority for detailed investigation with pressurized mercury as a lubricant. Available technical data was compiled and evaluated in order to establish the most compatible materials for bearing components.

Preliminary test runs with a fitted ball and socket on the Feasibility Bearing Test Rig proved the feasibility of the hydrosphere and indicated considerable thrust load capacity. The mounting design and the thermal expansion problems of the test rig however proved unsatisfactory for further testing, required to demonstrate conclusively the bearing capabilities.

The Feasibility bearing test rig was redesigned in order to eliminate mounting and thermal problems, provide additional instrumentation, and to provide for the application of radial loads. This modified Bearing Test Rig (MBTR) was used to test single hydrosphere bearings to gain parametric knowledge for correlation with design equations.

The Free Running Bearing Test Rig (FRR) was designed, fabricated, and assembled. This rig was intended to simulate the dual bearing construction of the final application with a hydrosphere bearing on either end of a shaft and was complete with the required auxiliary equipment and instrumentation.

Since results of the experimental testing performed on these rigs were the foundation for the final design of the SNAP I power system hydrosphere bearings, a detailed discussion of the experimental results of the tests is presented in Section 6.0 and a full description of the MBTR and the FRR is given in Section 10.0.

4.4 Hydrosphere Bearing Types

The original bearing type utilized perfectly mated spheres and sockets with axial grooves placed at 90° intervals around the bearing. The axial grooves were incorporated based on the belief that the resultant pressure distribution would provide the maximum thrust load capacity. However, after several low speed startup failures it was determined that the tightness of the bearing was detrimental to the radial load capacity since it would not allow the bearing to run eccentric and provide hydrodynamic pressure buildup. To alleviate this, the bearing was provided with an initial radial clearance of approximately .0001 in. After several apparent high speed radial load failures it was furthermore determined that the grooves were relieving the hydrodynamic pressure buildup in the loaded area. This development resulted in the elimination of the bearing grooves.

Further development testing and a two dimensional photo-elastic study resulted in the socket configuration shown in Figure 4-2.

4.5 Materials

Initial materials selection was based on the work of C. L. Goodzeit of the General Motors Research Center (3). On the basis of this study, Blue Chip, a Tungsten alloy high speed tool steel, 18-4-1, was selected as the base material for both ball and socket.

During the experimental hydrosphere bearing development, several bearing materials and plating combinations were tested. Flaking, cracking, and spalling of the platings resulted in elimination of platings as a bearing surface. The final basic material combination for the experimental development program was Blue Chip spheres in Blue Chip sockets.

Anti-scoring tests of 10 bearing material pairs were conducted under a subcontract to New Departure to determine the most promising materials in comparison with Blue Chip on Blue Chip.

A more detailed discussion of the Materials Development is included in Section 8.0.

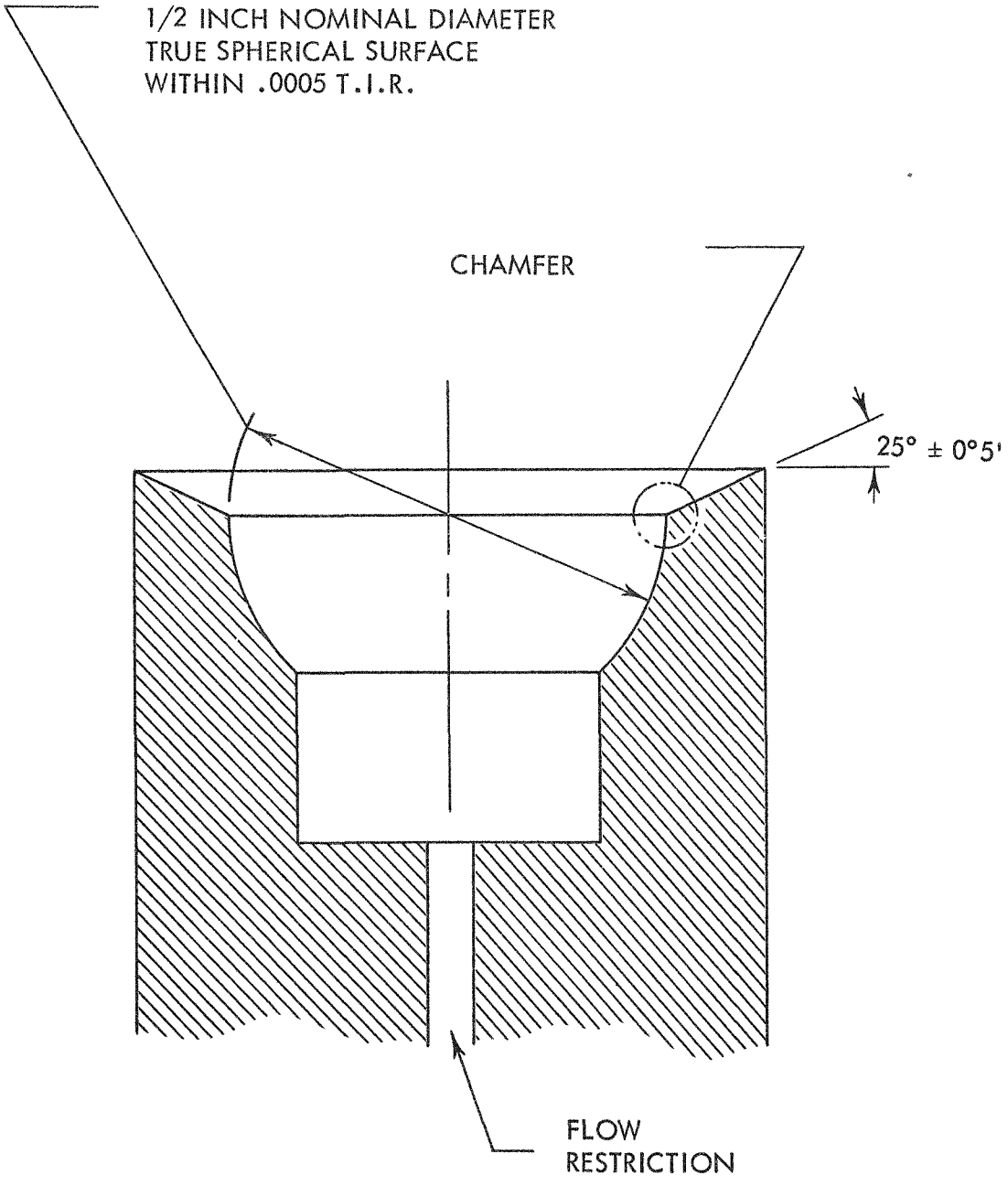

HYDROSPHERE BEARING SOCKET CONFIGURATION

FIGURE 4-2

5.0 HYDROSPHERE DESIGN ANALYSIS

5.1 Analytical Approach

As indicated earlier a rigorous mathematical analysis of the hydrosphere is complicated by the three-dimensional film which cannot be simply described. Moreover, the nonwetting and high density characteristics of mercury cannot be easily handled in the classical hydrodynamic bearing equations. Because of these complexities and the necessity to formulate parametric relationships at an early date, emphasis was placed on development by experiment along with analysis.

Parametric relationships were obtained by considering only the axi-symmetric configuration of the hydrosphere with the variable geometric parameter being the axial displacement of the ball out of the socket. Ball rotation effects were ignored, except in the analysis of bearing power. In addition, the classical assumptions of a wetting, Newtonian, constant viscosity, low density fluid were assumed. In this manner first order parametric relationships were derived. By analogy to cylindrical journal bearings and by test results, these approximate relationships proved useful in design and in prediction of hydrosphere performance.

In the derivations of the equations cognizance was given to the fact that in practice:

$$0 \leq \ell' \leq .040$$

$$0 \leq c' \leq .002$$

Wherever valid, the approximations:

$$1 \pm \ell'^2 \approx 1 \pm c' \approx 1.0$$

were used.

5.2 Film Geometry

The axi-symmetric configuration greatly simplifies the mathematical description of the film, although it is valid only in the no radial load condition. The clearance space between the spherical ball and the slightly larger hemispherical socket constitutes the film as shown in Figure 3-1. The film geometry is a function not only of the difference in ball and socket radii, but of the axial displacement between their centers. Zero displacement is defined as the concentric position and only outward displacement is considered.

Examination of Figure 3-1 will show that the film thickness ratio can be expressed as:

$$h' = \frac{h}{R} = 1/2\left[z^2 + 2z + (2c' - \ell'^2)\right] = 1/2\ Z \tag{5.1}$$

where $$z = \ell' \cos\theta \tag{5.2}$$

At the equator the maximum angle θ_m is defined, for all practical purposes, as:

$$\cos\theta_m = \ell' \tag{5.3}$$

The inlet angle θ_o can be expressed as:

$$\cos\theta_o \quad \frac{\ell' + \cos\phi_o}{1 + 2\ell'\cos\phi_o} \tag{5.4}$$

5.3 Pressure Distribution

The axi-symmetric pressure distribution in the film was derived assuming laminar flow in the axial direction only. The effects of ball rotation were ignored. With these assumptions the expression for film pressure was derived to be:

$$P - P_o = \frac{6\mu\ Q}{\pi R^2}\ (K_P - K_{P_o}) \tag{5.5}$$

where

$$(K_p - K_{p'_o}) = 32\ \ell \int_{z_o}^{z} \frac{dz}{(\ell'^2 - z^2)(4 - Z)Z^3} \tag{5.6}$$

$$= \frac{\ell'}{\ell'^2 - c'^2}\left\{\left[1 + \alpha(1 + z)\right]\frac{1}{Z^2} - \left[\frac{3}{2}\alpha + \beta(1 + z) + \frac{2c'}{\ell'^2 - c'^2}\right]\frac{1}{Z}\right. \tag{5.7}$$

$$+\left[\frac{3}{2}\alpha + \beta + \frac{c'(3 - c') + \ell'^2(1 - 3c')}{\ell'^2 - c'^2}\right]\frac{1}{2\gamma}\ln\frac{1 + z + \gamma}{1 + z - \gamma}$$

$$\left. + \frac{1}{4\ell'(\ell'^2 - c'^2)}\left[(\ell' + c')^3 \ln\frac{(\ell' + z)^2}{Z} + (\ell' - c')^3 \ln\frac{(\ell' - z^2)}{Z}\right]\right\}$$

where $$\gamma^2 = 1 - 2c' + \ell'^2 \tag{5.8}$$

$$\alpha = \frac{1 - c'}{\gamma^2} \tag{5.9}$$

$$\beta = \frac{1 - c'^2 - \quad ^2}{\gamma^2(\ell'^2 - c'^2)} \tag{5.10}$$

Figure 5-1 shows typical pressure distribution curves obtained from equation (5.5).

5.4 Flow

Essentially, the hydrosphere is a variable flow restriction coupled with a fixed restriction. Thus, lubricant flow is an important parameter directly related to pressure distribution, which, in turn, is related to axial load capacity. Rearrangement of equation (5.5) and substitution of the conditions at the equator or discharge area Yields:

$$Q = \frac{\pi R^3}{6\mu} (P_m - P_o) K_Q \tag{5.11}$$

where $$\frac{1}{K_Q} = 32\ell' \int_{z_o}^{z_m} \frac{dz}{(\ell'^2 - z^2)(4 - Z) Z^3} \tag{5.12}$$

In terms of weight flow in pounds per minute the flow factor can be expressed as:

$$K_Q = 8.25 \times 10^{-5} \frac{\nu \dot{w}}{R^3 (P_o - P_m)} \tag{5.13}$$

Figure 5-2 shows typical curves derived from equation (5.11). This equation, when plotted for different values of inlet angle, ϕ_o, shows that the value of ϕ_o has very little effect on flow.

5.5 Axial Load Capacity

The axial load capacity of the axi-symmetric hydrosphere is obtained by integration of the pressure forces acting on the ball. By integrating the axial components of the pressure forces the axial load capacity factor can be shown to be:

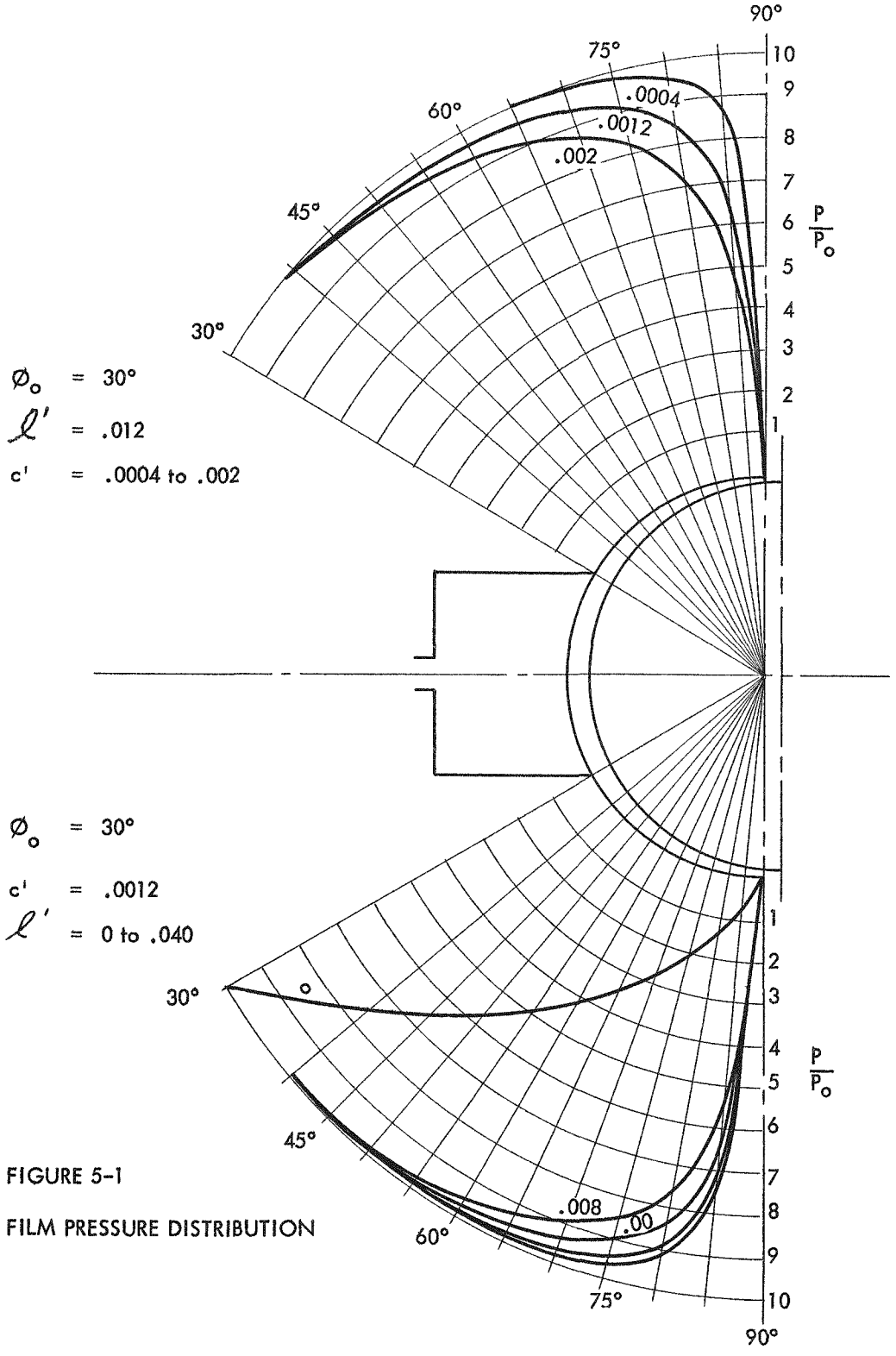

FIGURE 5-1

FILM PRESSURE DISTRIBUTION

FIGURE 5-2

EFFECT OF LIFT ON FLOW

C' = .0004 to .002 ϕ_o = 30°

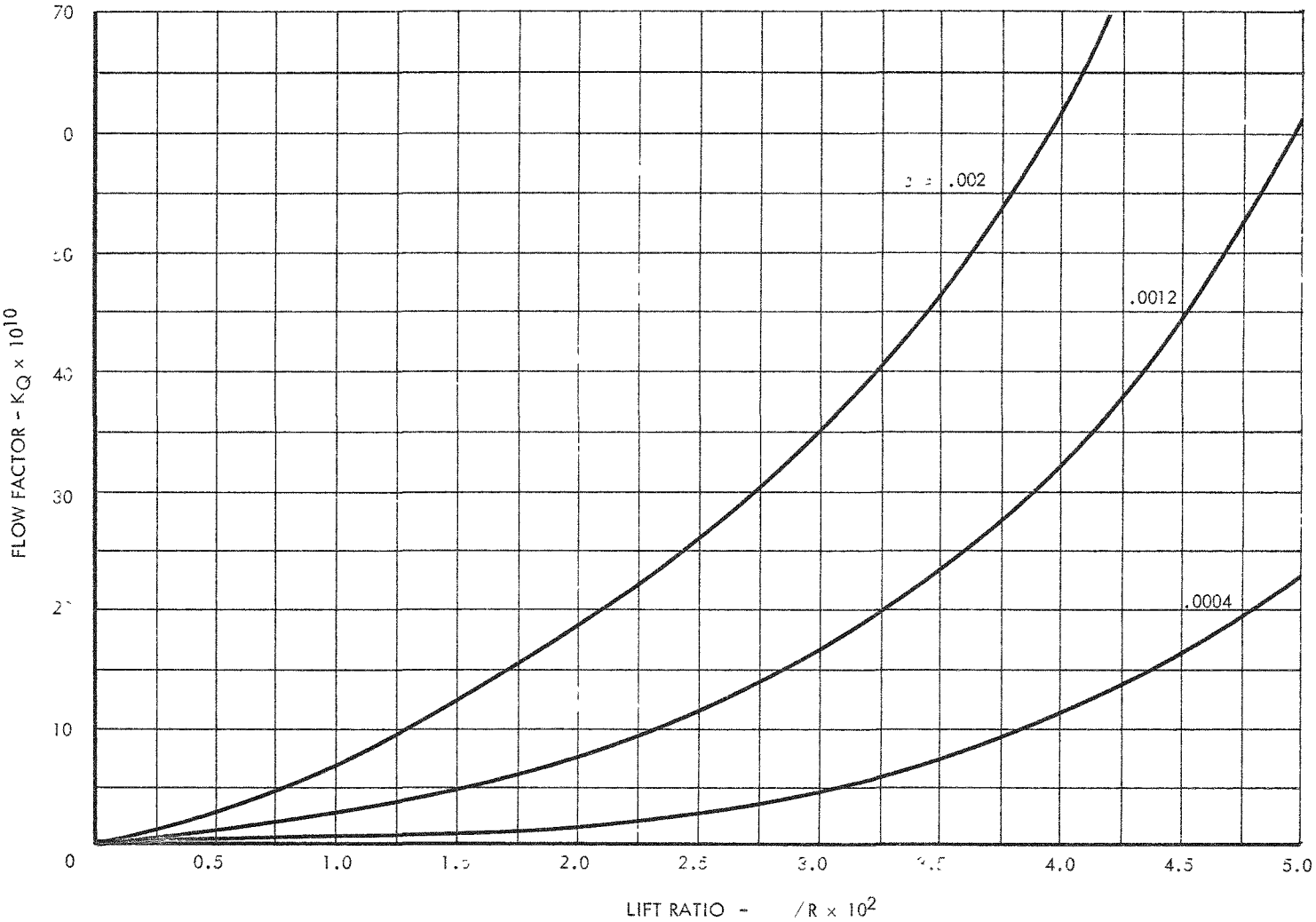

FIGURE 5-2

$$K_A = \frac{W_t}{\pi R^2 (P_o - P_m)} \qquad (5.14)$$

$$= 1 + \frac{2K_Q}{\ell'^2} \int_{z_o}^{z_m} (K_{p_o})\, Z dZ$$

$$- \frac{\ell'}{(1 - P_m/P_o)} \left(\frac{2 \cos \phi_o \sin^2 \phi_o}{1 + 2\ell' \cos \phi_o} \right) \qquad (5.15)$$

Consideration of the order of magnitudes for the second two terms on the right hand side of equation (5.15) for practical ranges of values for ℓ', c', ϕ_o, P_m , and P_o show that:

$$K_A \approx 1 \qquad (5.16)$$

5.6 Radial Load Capacity

To sustain a radial load, the hydrosphere must have a film pressure distribution which is unsymmetrical about its axis. Unfortunately, the mathematical description for the film thickness of a radially and axially displaced ball is extremely unwieldy. Even an expression for the simpler hydrostatic radial load capacity becomes practically underivable. The added consideration of ball rotation for the hydrodynamic case makes this solution formidable. The empirical relationship suggested by Shaw and Macks was therefore used. This expression has no analytical basis, but was suggested by their test observations.

$$W_R \leq \frac{1}{2} W_t \qquad (5.17)$$

It was obvious that speed, lubricant temperature, surface finish, and socket pressure would affect radial load capacity, so that equation (5.17) was used as a limit value rather than a prediction of capacity.

5.7 Power Loss

In addition to its dual load capacity, its low power loss was a major factor in the original selection of the hydrosphere. The low power loss was originally predicted from a simplified analysis. Early test results, however, showed higher power consumption and indicated the need for a more refined expression for bearing power loss.

The derivation for this expression assumes the axi-symmetric case and considers only circumferential flow. The assumption is analogous to the Petroff condition in classical cylindrical journal bearing analysis. It should be noted that in the case of the axi-symmetric hydrosphere,

power loss decreases with increasing lift (i.e., increasing film thickness). Practically, this reduction in power loss may not be realized in a radially loaded bearing which will not be axi-symmetric. In practical journal bearings it can be shown that power loss may be insensitive to comparatively large changes in radial clearance, if all other conditions are held constant. However, as in cylindrical journal bearing analysis, the axi-symmetric case yields useable initial estimates of hydrosphere power loss.

Applying the assumptions previously outlined the expression for power loss in the axi-symmetric case was derived to be:

$$H = 7.8 \times 10^{-3} \mu R^3 N^2 K_T \tag{5.18}$$

where

$$K_T = \frac{2}{\ell'^3} \int_{z_o}^{z_m} \frac{(z^2 - \ell'^2)\, dz}{Z} \tag{5.19}$$

$$= \frac{2}{\ell'^3} \left[(z_m - z_o) + \ln \frac{z_o}{z_m} - \alpha \ln \left(\frac{1 + z_o - \gamma}{1 + z_o + \gamma} \quad \frac{1 + z_m + \gamma}{1 + z_m - \gamma} \right) \right] \tag{5.20}$$

In addition to the problems arising from the assumption of axial symmetry, equation (5.19) becomes indeterminate when $\ell' = 0$. Moreover, as $\ell' \to 0$ the precision of the numerical values for each of the three terms will have a great effect on the accuracy of the answers. The first term is of the order of the algebraic sum of the last two terms.

For the case of $\ell' = 0$, equation (5.19) reduces to

$$K_{T_o} = \frac{2}{c'} \int_0^{90^\circ} \sin^3 \phi \; d\phi \tag{5.21}$$

$$= \frac{\cos \phi_o}{3c'} (3 - \cos^2 \phi_o) \tag{5.22}$$

Figure 5-3 shows the effect of lift on power loss of axi-symmetric hydrospheres.

5.8 Two Dimensional Photo-Elastic Study of Hydrosphere Contact Stresses

One of the desired features of the hydrosphere bearing in the SNAP I application is a capability to withstand unpressurized starts without scoring or seizure. Because of the point contact which exists between the ball and its mating socket until the hydrodynamic and hydrostatic pressures are capable of supporting the radial load, and because of the geometric discontinuity at the point of contact, the Hertz pressures can be quite large.

FIGURE 5-3

EFFECT OF LIFT ON FRACTIONAL TORQUE AND POWER

C' = .0002 to .005 ϕ_o = 30°

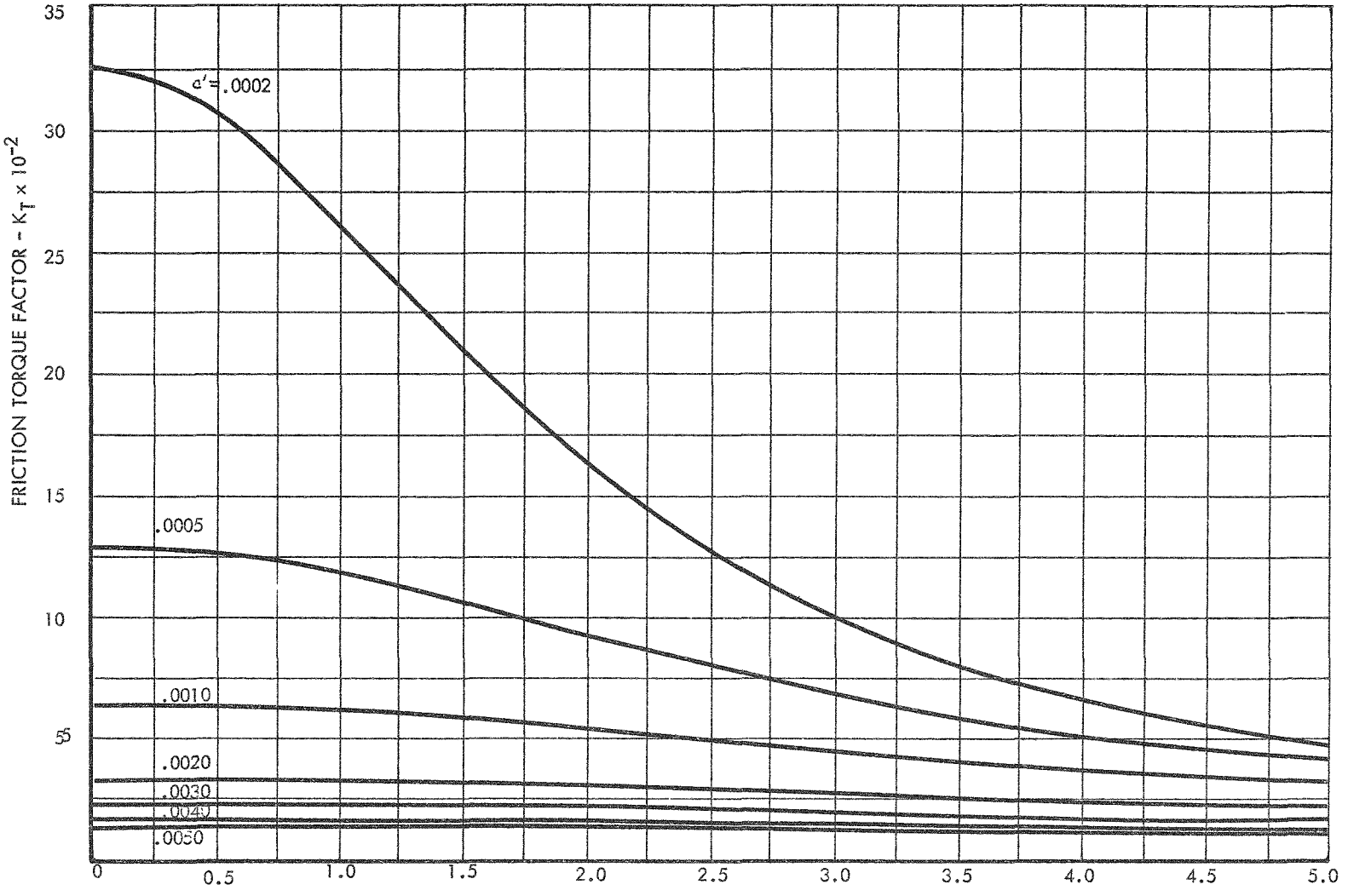

FIGURE 5-3

Although the proper selection of materials may provide adequate scoring and seizure resistance, the determination of the magnitude of the Hertz contact pressures is necessary to insure that no permanent deformation occurs.

The objectives of this investigation were:

1. To evaluate the stress change resulting from a cylindrical extension of the socket beyond the equator, and

2. To establish a stress concentration factor to be applied to the formula for calculating contact pressures.

The discontinuity at or near the point of contact makes mathematical determination of the stress magnitude difficult, if not impossible. Photoelasticity provides a comparatively simple method, particularly when two-dimensional models are used. The problems associated with the equipment and procedures of three-dimensional photoelasticity and the belief that the two-dimensional study was adequate for the desired purpose led to the selection of the latter method.

The fabrication, loading and photographing of the models were done at the Case Institute of Technology by Professor Daniel K. Wright, Jr. Professor Wright also evaluated the results of the study and provided the necessary calculations related to the photoelastic investigation.

The two-dimensional photoelastic study included investigation of three socket configurations to determine the effect of a cylindrical extension beyond the socket equator as shown in Figure 5-4. From the results of the study, the following conclusions were drawn:

1. An extension of the socket to 1/32 inch beyond the equator reduces the Hertz contact pressure to approximately 43% of that encountered without the extension.

2. Increasing the extension beyond 1/32 inch does not result in further significant reduction of the contact pressure.

3. Modification of the socket extension by the addition of a radius or a 45° chamfer which does not extend into the contact area, as shown in the magnified view on Figure 5-4, does not change the contact pressure induced in the extended configuration.

4. Reasonable approximations for the magnitude of the Hertz contact pressure induced in the hydrosphere are:

    a. For the unextended configuration, 100% of the calculated pressure for a sphere on a flat plate.

TWO-DIMENSIONAL PHOTOELASTIC MODEL

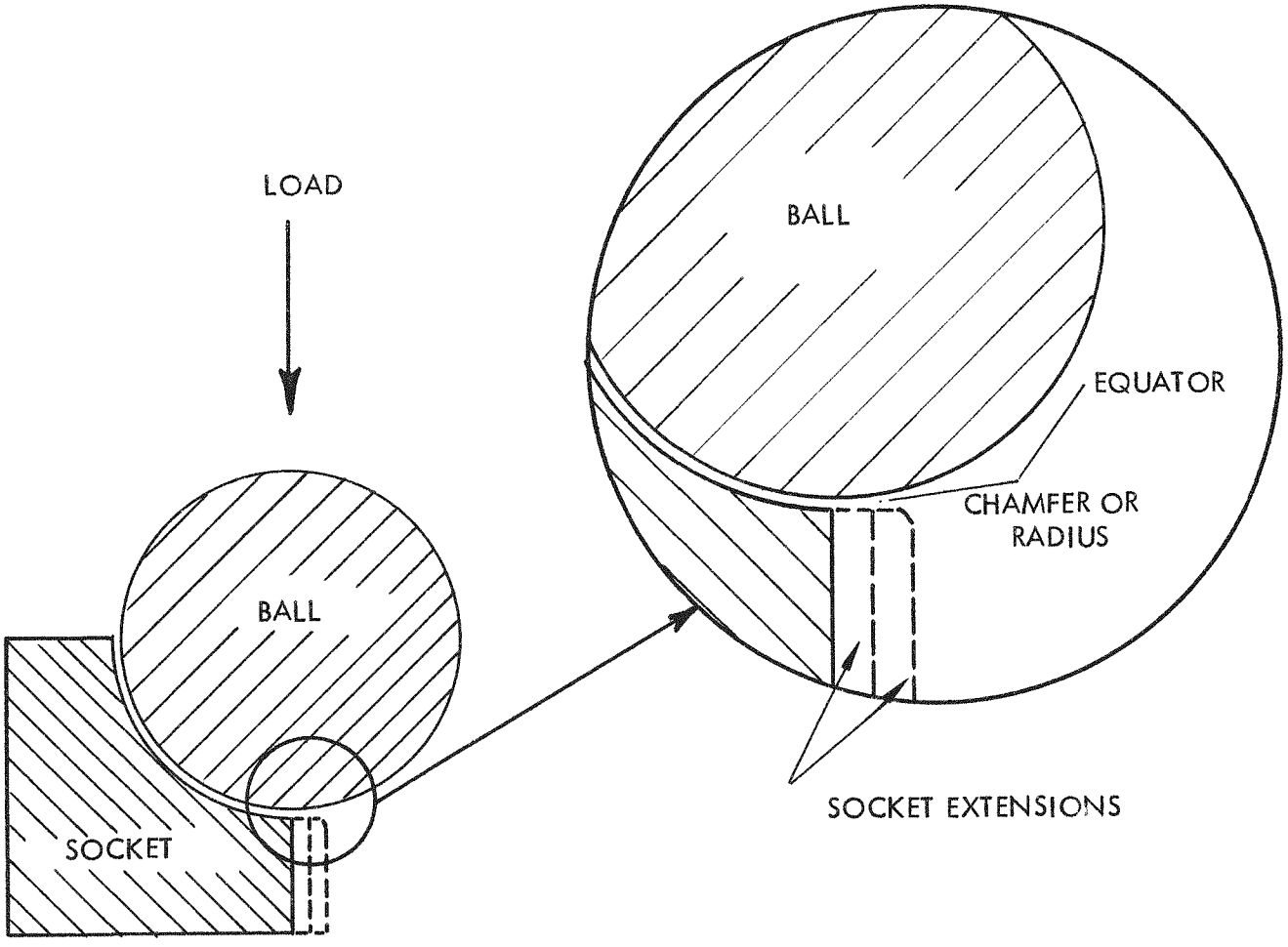

FIGURE 5-4

b. For the extended socket, 43% of the flat plate value.

Startup conditions, anticipated momentary overloads, and transportation shock and vibration require that the bearing be able to withstand metal-to-metal contact without damage. One criterion of scoring and wear damage is the product of contact pressure and the rubbing velocity. Since the shaft speed for the application under consideration is dictated by other requirements, the rubbing velocity can be reduced only by decreasing the bearing diameter. A smaller diameter, however, results in lower radial load capacity and in higher contact pressures. A second solution is to modify the socket configuration as indicated by the results of the photoelastic investigation. With a proper chamfer or radius, the proposed configuration is amenable to fabrication methods and bearing performance is not affected.

6.0 HYDROSPHERE BEARING CHARACTERISTICS

Due to the lack of adequate theoretical analysis in the early phases of the program, the development effort was directed to determination of the design parameters and obtaining an experimental evaluation of the hydrosphere bearings. The Modified Bearing Test Rig was utilized to obtain the single hydrosphere bearing parameters necessary to correlate theoretical relationships. This information was also used as a basis for the improvement of single and dual bearing operating characteristics.

Since the data obtained on the MBTR and the FRR were in close agreement and since the end product of the development program was a dual bearing shaft, the remainder of this section deals primarily with information obtained from tests in the Free Running Bearing Test Rig.

6.1 Flow

The flow of mercury lubricant to the bearing was controlled by flow restrictions upstream of the bearings and by the axial and radial clearance of the bearings. The interdependency of flow on both axial and radial clearance is shown in Figures 6-1 and 6-2. This type of curve was used to evaluate the conditions of the bearing surfaces before and after dynamic testing. Any shifting of this curve indicates scoring, change of axial clearance, film buildup, etc. A comparison between theoretical and actual flow versus lift at various clearances is shown in Figure 6-3. The deviation is attributed to the fact that the theoretical curve is based on concentric radial clearance while the actual data is generated for the eccentric case which results in higher flow rates.

The importance of maintaining sufficient lubricant flow is seen in Figure 6-4. If the flow rate per bearing becomes less than $\approx$ 3.0 lbs/min, the resultant heat rise may add to the thermal expansion problem which is already present. The likelihood of film cavitation is also increased by the large temperature rise. The system requires that the lubricant flow be 10.0 lbs/min. Therefore, in order to satisfy the system and the bearings the total lubricant flow must be $>$ 6.0 and $<$ 10.0 lbs/min.

6.2 Flow Restrictions

A flow restriction upstream of the socket was an integral part of the hydrosphere bearing assembly to accommodate changing axial loads. In the SNAP I package, constructional and system problems prevented the use of laminar flow restrictions. The following paragraphs discuss the types that were used.

6.2.1 Fixed

In the preliminary component and prototype test packages, the flow to the bearings was controlled by fixed flow restrictions located between the reservoir and the bearings. The

HYDROSTATIC FLOW CALIBRATION AT VARIOUS AXIAL CLEARANCES

RADIAL CLEARANCE = .0001/.00015 INLET DIAMETER - .250" ϕ_o = 30°

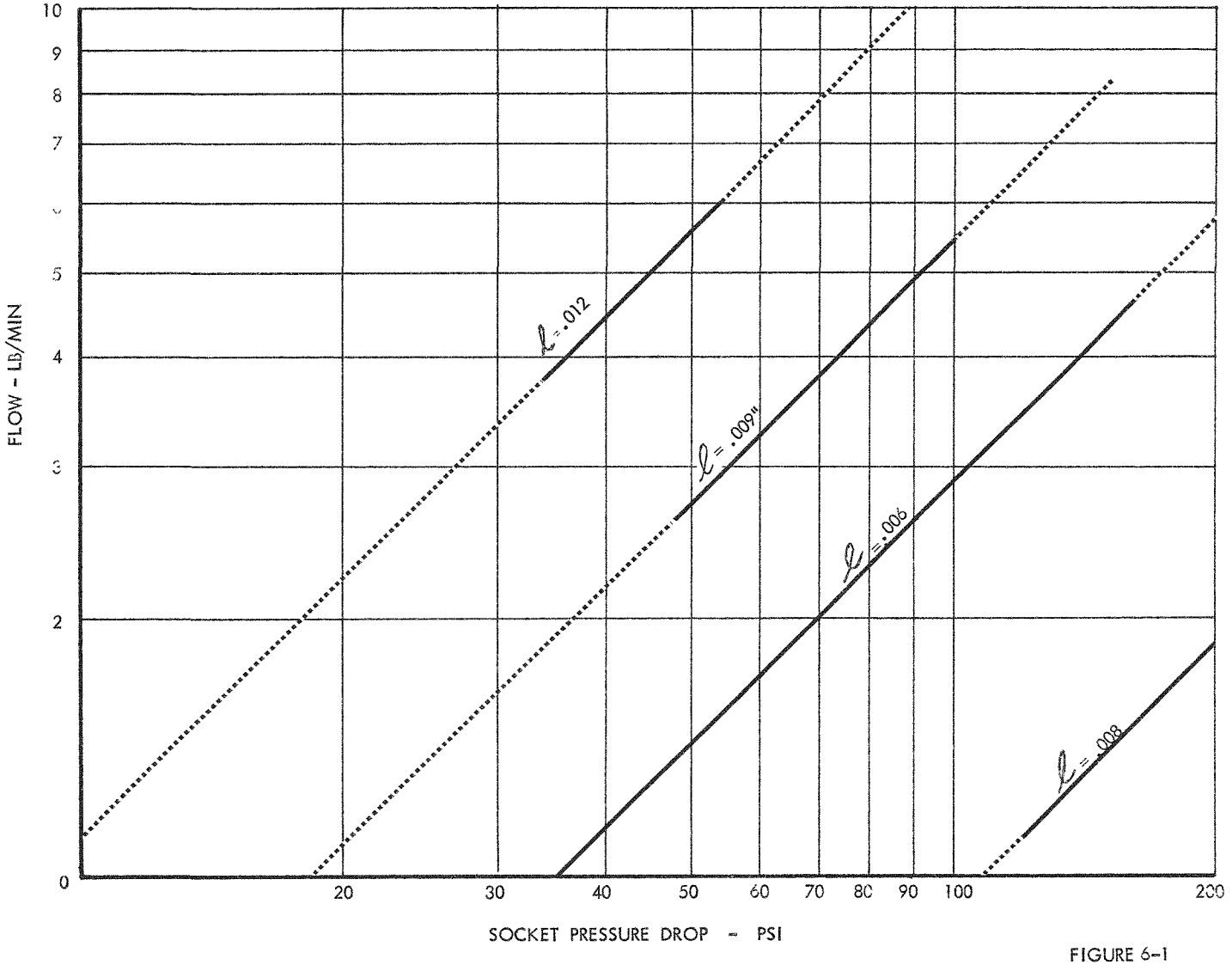

FIGURE 6-1

HYDROSTATIC FLOW CALIBRATION AT VARIOUS RADIAL CLEARANCES

TOTAL AXIAL CLEARANCE = .008 INLET DIAMETER = .250 $\phi_o = 30°$

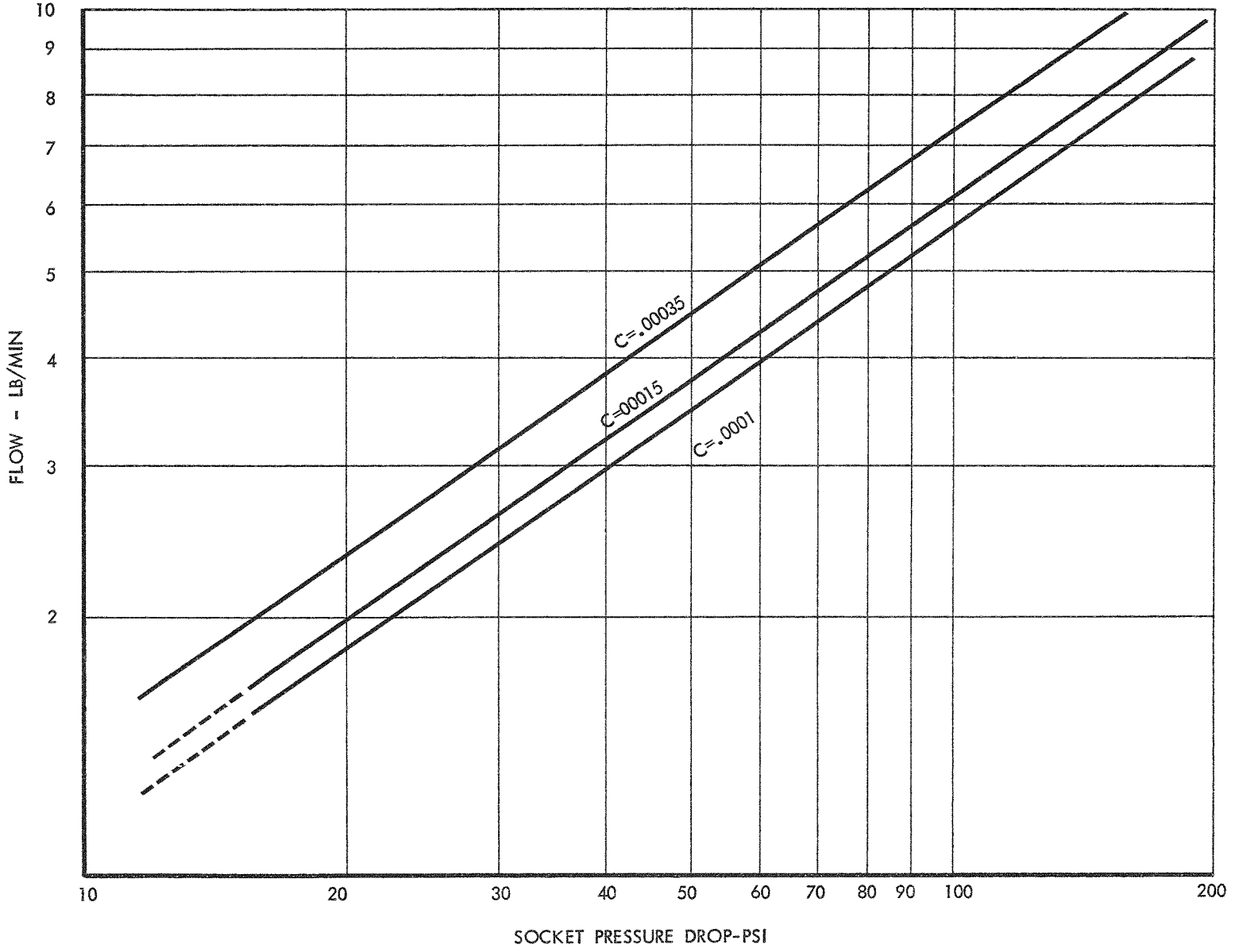

FIGURE 6-2

EFFECT OF LIFT ON FLOW

C' = .0001 - .0006 $\emptyset_o$ = 45°

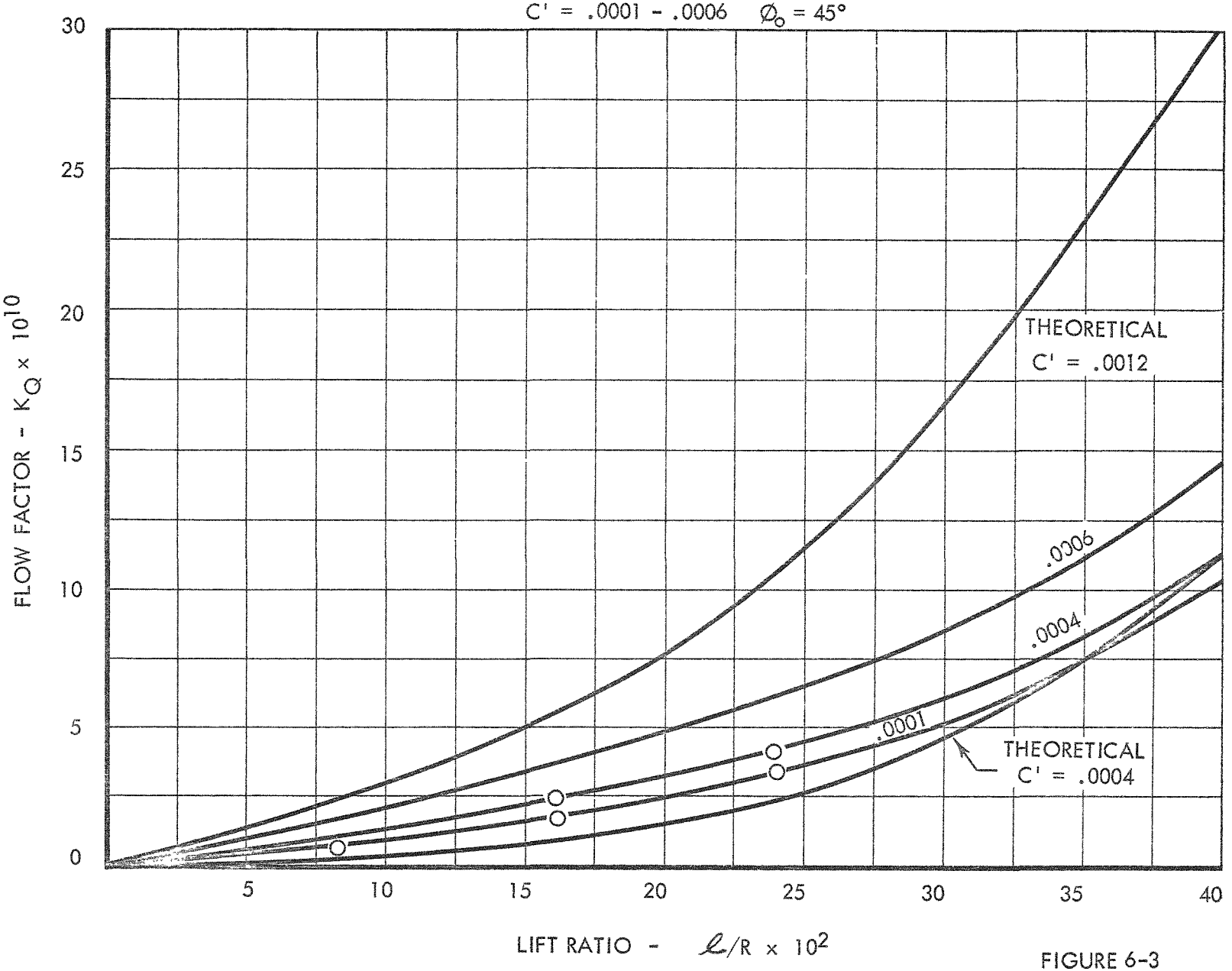

FIGURE 6-3

MERCURY FLOW VERSUS TEMPERATURE RISE

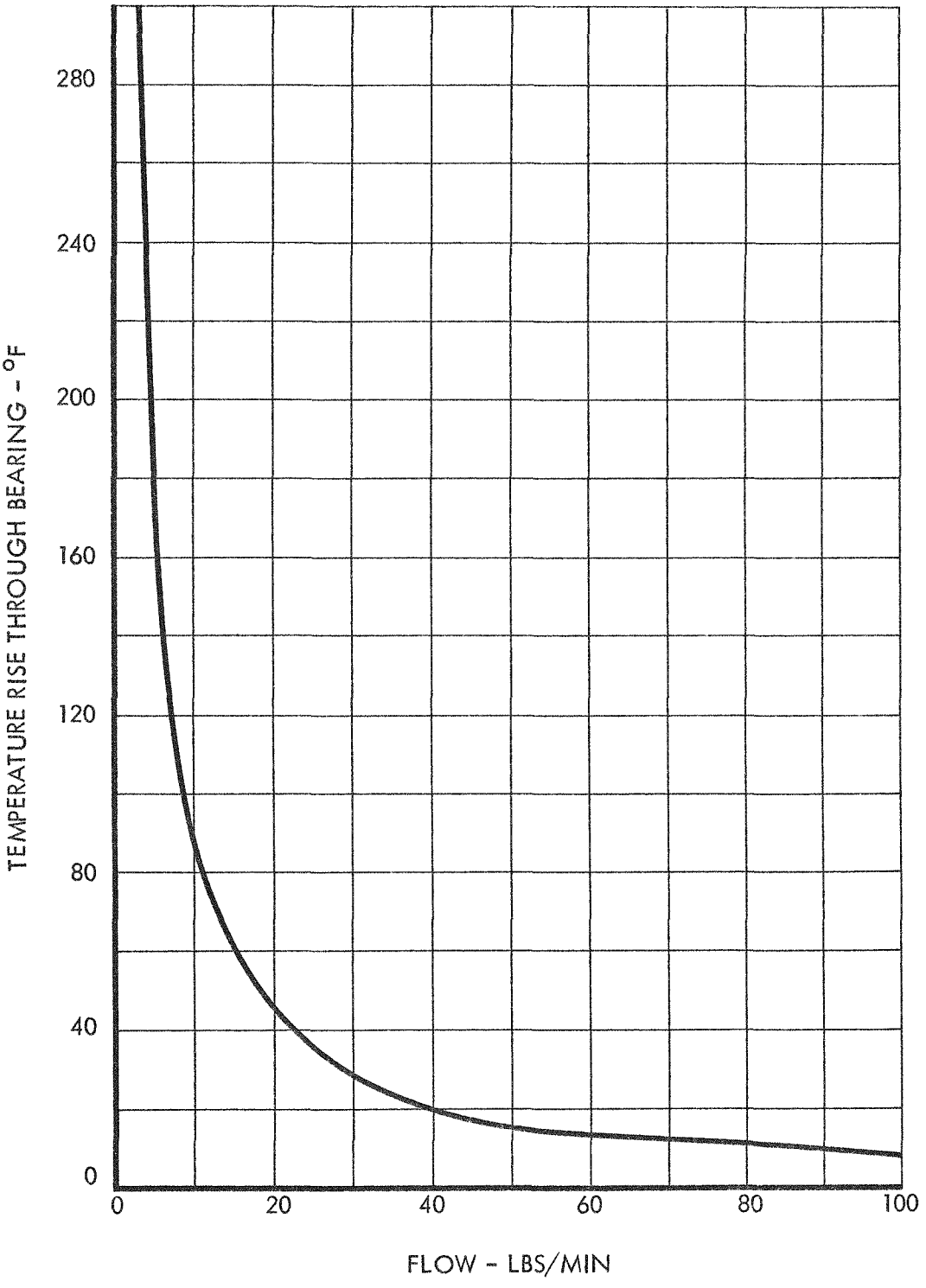

FIGURE 6-4

fixed flow restrictions were calibrated by measuring the weight flow of mercury for a specific length of time at various pressure drops across the restriction. Figure 6-5 is a calibration of the various fixed flow restrictions that were used. A good approximation of the flow is obtained from the equation:

$$\dot{w} = C \sqrt{P_s - P_o} \qquad (6.1)$$

6.2.2 Annular; Static

Since the incorporation of the jet-centrifugal pump outboard of the alternator bearing complicated the thrust capacity and leakage path of the bearing, a redesign of the flow restriction was necessitated. Analysis indicated that the best solution was an annulus between the pump shaft and the bearing housing.

The theoretical flow vs pressure drop relationship was set up on the IBM 610 computer and the results are shown in Figure 6-6. The correlation of actual data with these theoretical curves is also shown by Figure 6-6.

6.2.3 Annular; Dynamic

The static data presented in the previous section was not sufficient to predict or analyze dynamic test results. The interdependency of the bearing inlet flow and pump cavity pressure, which is a function of speed, prohibited dynamic annulus calibration of a pump-bearing unit. Therefore, a unit with an extended shaft, but without a pump was tested. From these results it was determined that if the static calibration of an annulus was reduced by 30% a good correlation of flow at design speed existed. This relationship was used for the remainder of the program in predicting and analyzing test results.

6.3 Power Loss

The most reliable power loss data was obtained from spindown test of the FRR and package units. The relationship used to obtain power loss from such deceleration tests was

$$T_B = I\alpha - K_W N^{1.8} \qquad (6.2)$$

where the second term on the right side of the equation represents the windage torque on the shaft assembly. To obtain bearing power loss, the deceleration was determined from speed time data obtained from the spindown and the windage torque was calculated.

A typical power loss curve for a 1/2 inch diameter hydrosphere is shown as Figure 6-7.

6.4 Thrust Load

The thrust load capacity of a dual hydrosphere system has been shown experimentally to approach the value obtained by the following equation:

FLOW RATIO VERSUS PRESSURE DROP ACROSS FIXED FLOW RESTRICTION
P_o = SOCKET PRESSURE

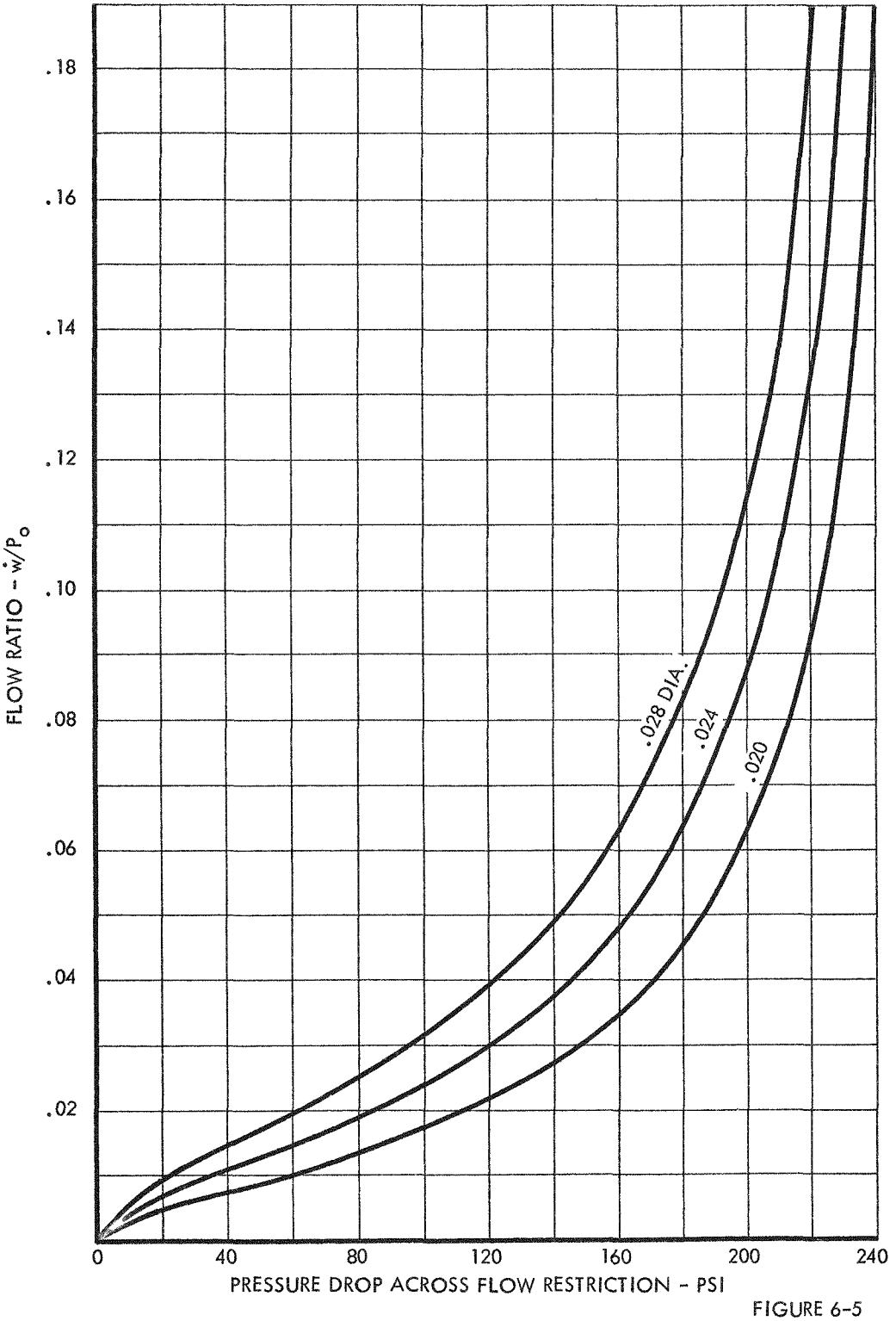

FIGURE 6-5

THEORETICAL FLOW THROUGH A CONCENTRIC ANNULAR FLOW RESTRICTION
VERSUS PRESSURE DROP AND ROOM TEMPERATURE

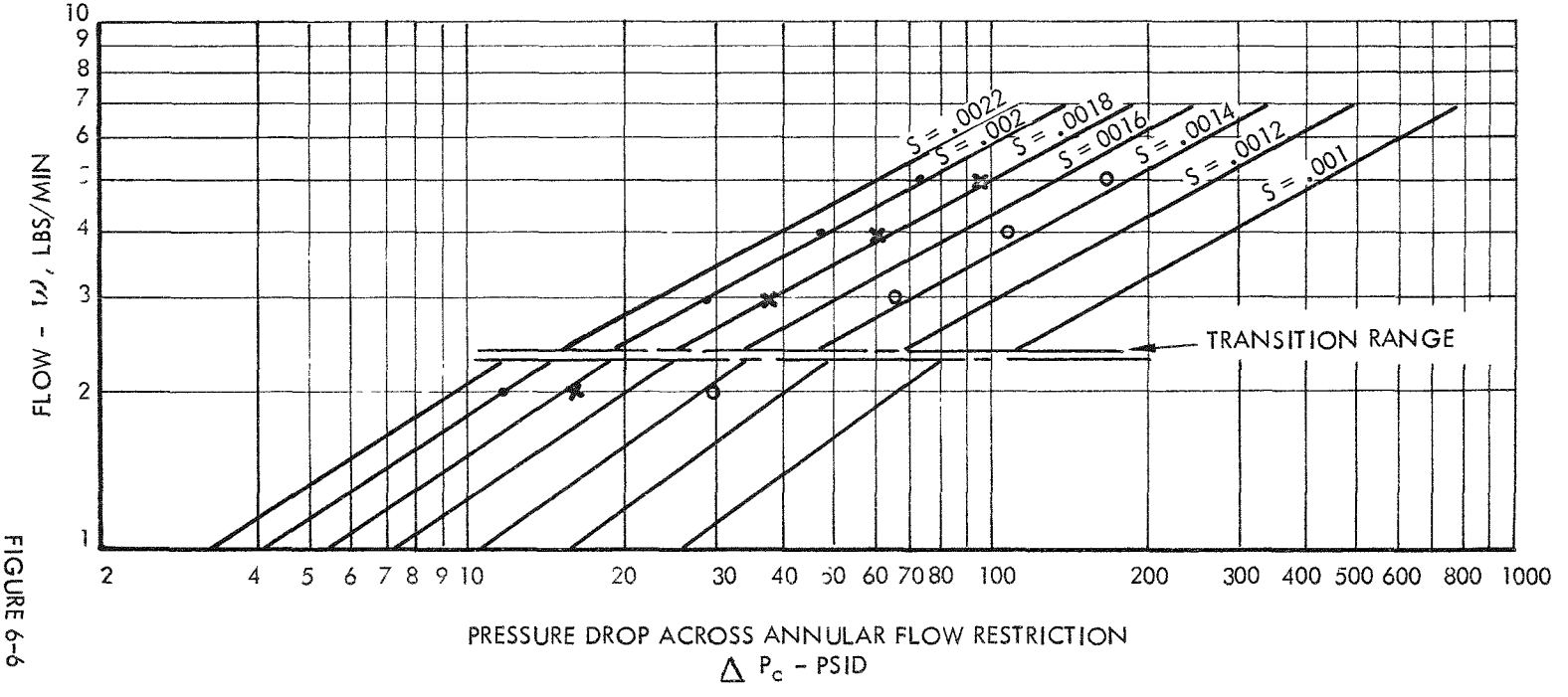

FIGURE 6-6

BEARING POWER LOSS VERSUS SPEED

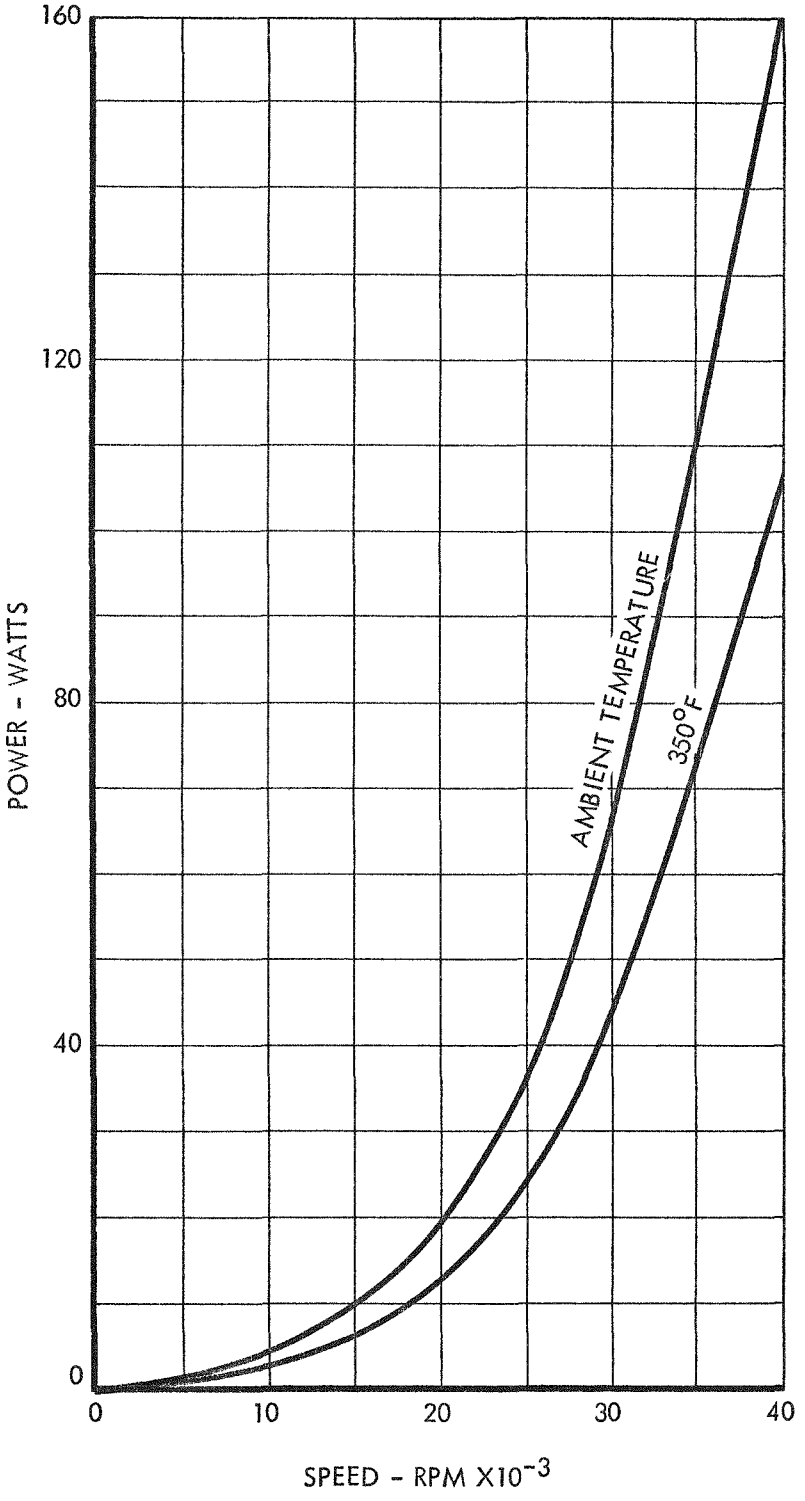

FIGURE 6-7

$$W_T = \pi R^2 (P_{oA} - P_{oB}) \qquad (6.3)$$

where A and B refer to the individual bearing socket pressures.

It is apparent from this equation that with a fixed diameter hydrosphere the maximum thrust capacity is dependent upon socket pressures which are in turn dictated by the choice of supply pressure and flow restrictions. The requirements of the SNAP I system resulted in a bearing whose demonstrated thrust capacity is in the range of 25-30 lb.

The addition of an extended shaft on which the system pump was mounted, outboard of the bearing, complicated the simple relationship shown above. However, the thrust capacity can still be adequately determined by the difference of the product of the respective cross sectional areas and bearing socket pressure. A typical thrust curve is shown as Figure 6-8.

6.5 Radial Load

The destructive characteristics of radial load capacity tests and the shortage of time and test specimens precluded absolute determination of this characteristic. However, FRR tests indicated 1/2 inch diameter dual bearing radial load capacities to 25 pounds. Other tests indicate that the bearing is also capable of hydrostatic radial load support.

6.6 Lubricant Temperature Rise

The monitoring of lubricant temperature rise was used in determining bearing power loss through a heat balance analysis. However, it was soon discovered that the complexity of the package housings and shaft resulted in thermal gradients which were difficult to determine and this method was disregarded. Temperature rise data was employed only to insure that the discharge temperature of the bearing was below the vaporization point.

6.7 System Contamination

The hydrosphere system is sensitive to clearance changes since a reduction in clearance of the flow restrictions or the bearings while running results in a corresponding reduction in load capacity. Therefore, the amount of system contaminants which might result in clearance changes should be minimized. An effective filter upstream of the bearings was also recommended to insure minimum admittance of contaminants into critical areas.

6.8 Bearing Life

Bearing life at design operating conditions is one of the most important considerations of the SNAP I system. The first endurance run of 48 hours was completed on the prototype turbo-machinery unit in the mercury breadboard test facility, and the 60 day life requirement was exceeded in the System Test Enclosure (STE) on the Ground Test System (GTS). This system accumulated 2510 hours of endurance testing and the test was terminated with

THRUST LOAD VERSUS SOCKET PRESSURE DIFFERENCE

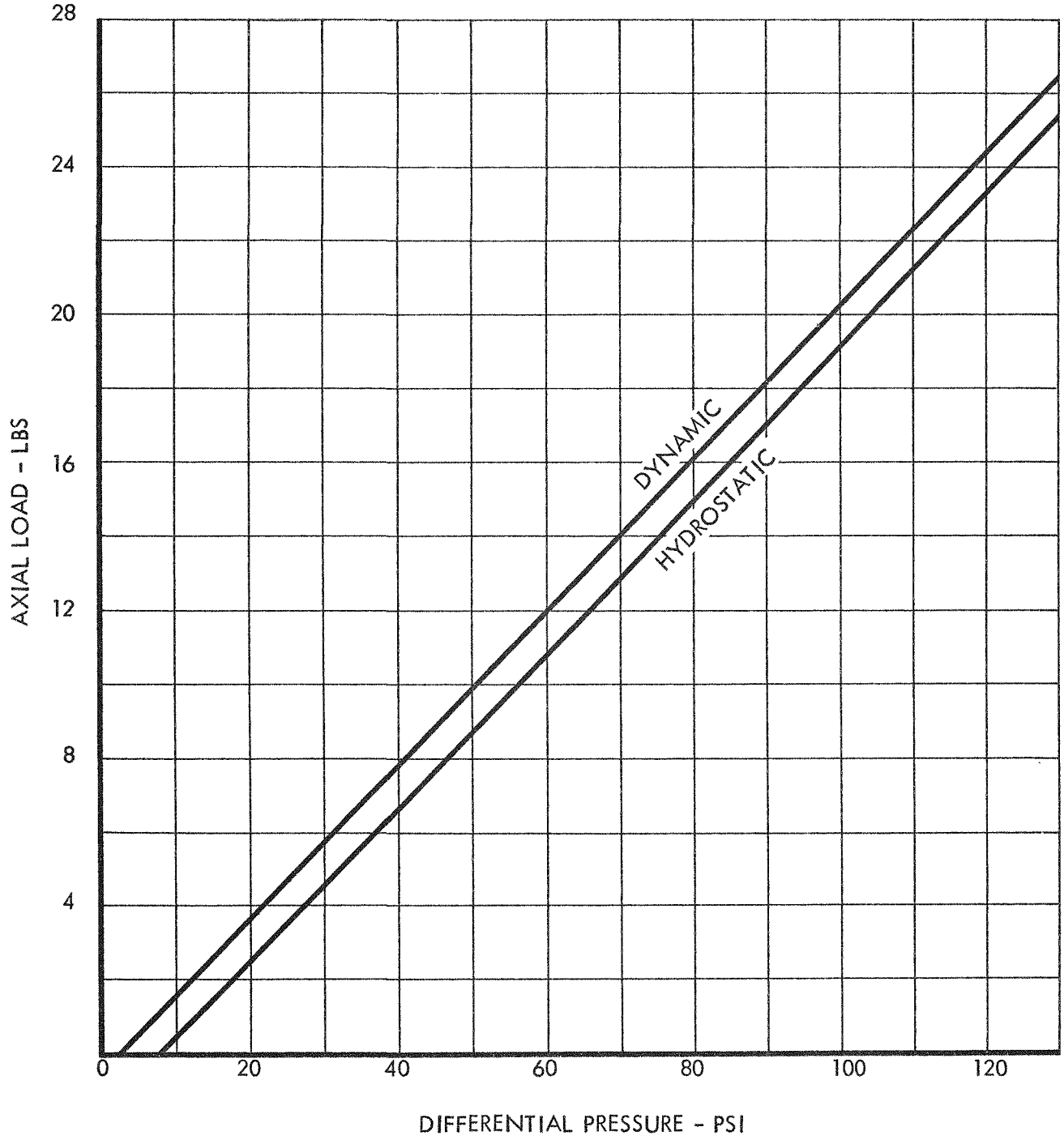

FIGURE 6-8

a planned shutdown without encountering any bearing malfunction. The composite performance of the 1/2 inch diameter hydrosphere bearings during these tests is typified in Figure 6-9.

COMPOSITE BEARING PERFORMANCE
DIAMETER = 1/2 INCH

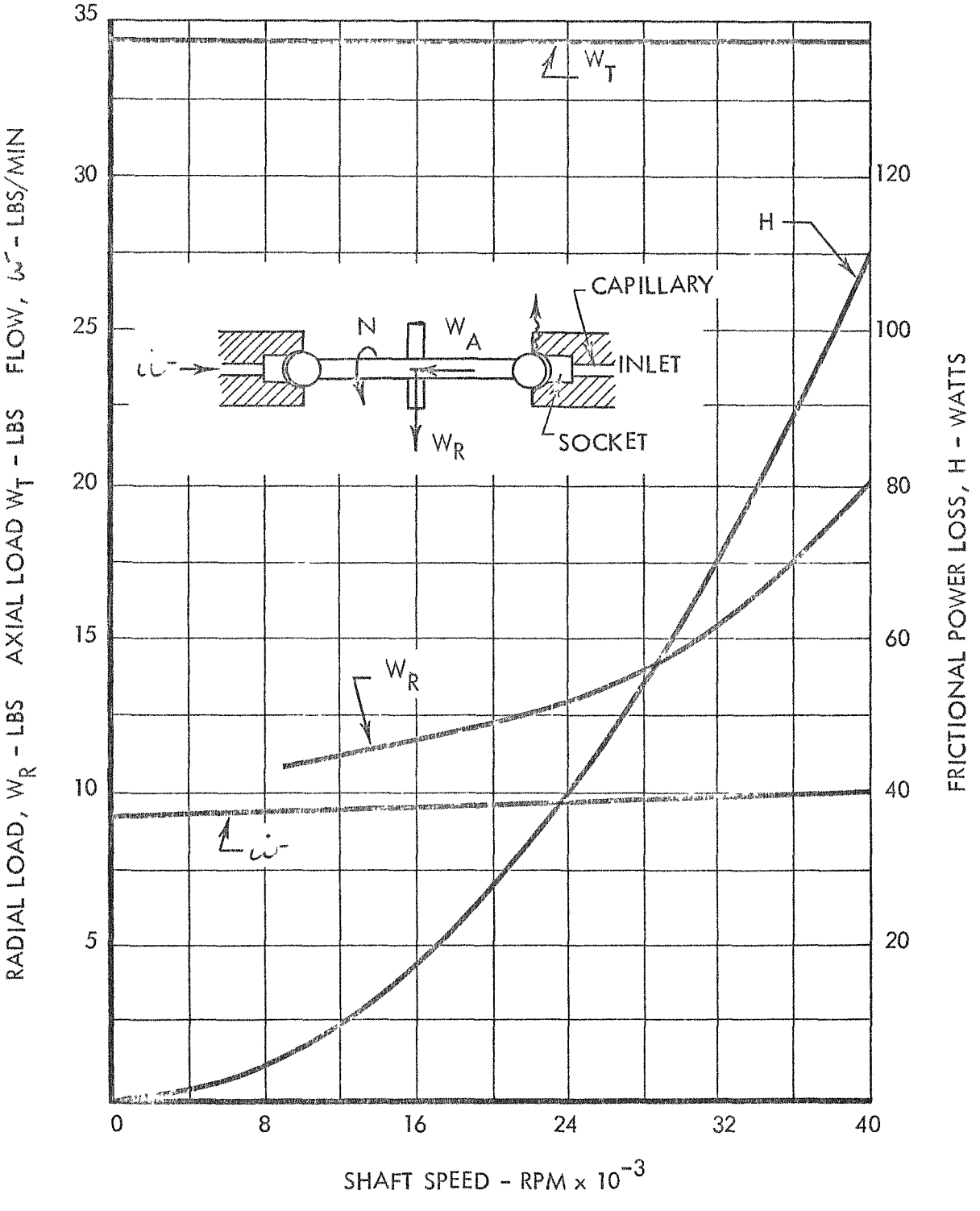

FIGURE 6-9

7.0 HYDROSPHERE BEARINGS IN TEST PACKAGES

Incorporation of the bearings in subsystem and system test packages followed the successful development of the hydrosphere bearings in component tests as discussed in the previous section. Extended shaft tests were necessary to obtain a satisfactory configuration and bearing characteristics prior to incorporation of the jet-centrifugal pump. These tests were followed by subsystem tests of the hydrosphere bearing-jet centrifugal pump combination in order to simulate final package configuration and to insure satisfactory bearing and pump operation while coupled. Integration of the bearings in the system test packages represented the culmination of a successful hydrosphere bearing development program.

7.1 Extended Shaft For Overhung Impeller

The addition of an extended shaft outboard of a hydrosphere bearing, necessitated by the centrifugal pump, produced configuration, thrust, and flow problems. A close clearance, nonrubbing, shaft seal was utilized to minimize leakage between the pump and bearing. Since this was not a positive seal, investigation of the magnitude, direction, and effect of the leakage on component performance and characteristics was required. The addition of the extended shaft on the pump and bearing reduced the thrust capacity of this bearing due to the reduction in area exposed to socket pressure. The utilization of a bearing supply annulus between the bearing annular orifice and the pump leakage seal was necessary to maximize bearing thrust capacity. The extended shaft and the flow passages were similar to those shown on the final pump-bearing configuration of Figure 7-1.

Extended shaft tests in the Free Running Bearing Test Rig indicated that satisfactory bearing thrust capability and flow characteristics could be obtained with this configuration. The static and dynamic flow characteristics of the bearing annular orifice were evaluated in these tests and are discussed in Section 6.2. The thrust capacity of the final extended shaft bearing and configuration is discussed in Section 6.4.

7.2 Hydrosphere Bearing-Jet Centrifugal Pump Subsystem

The Free Running Bearing Test Rig was modified to incorporate provisions to test a pump-bearing combination. The pump-bearing subsystem, as shown in Figure 7-1, is essentially a dual hydrosphere bearing assembly consisting of a shaft incorporating two hydrosphere bearings and a smaller diameter shaft extension with an end mounted radial impeller supplemented by the jet boost stage. The subsystem is powered by a Terry type air turbine mounted equidistant between the bearings. This test rig was used for the final evaluation of the Snap 1 pump and bearings before incorporation into the prototype package. The pump-hydrosphere bearing configuration presented conditions of operation which were unique to conventional pump-bearing systems and required special testing and analysis to investigate the following areas:

PUMP-BEARING COMBINATION TEST FIXTURE

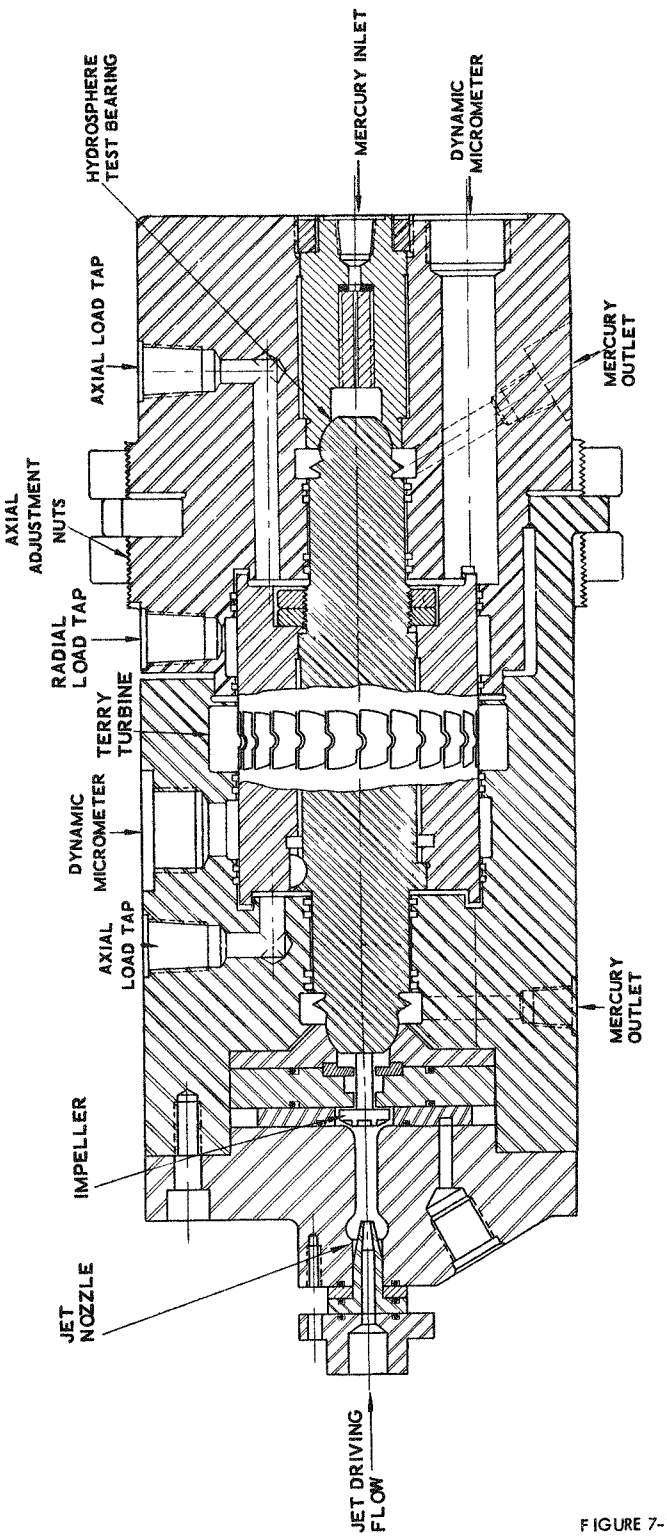

FIGURE 7-1

1. Axial location of the bearing shaft: Since the performance of the pump is sensitive to front face clearance, the effect of pre-set axial bearing clearance and pump thrust on axial clearance was required.

2. Effect of pump axial thrust: Demonstration of the ability of the bearings to support the thrust load of the pump plus simulated turbine thrust load was required in addition to maintaining proper front face clearance for the pump.

3. Leakage: The effect of mercury leakage into or out of the pump cavity on pump-bearing performance was required.

The pump-bearing subsystem operated satisfactorily both in separate hydraulic circuits and coupled together up to 45,000 rpm. Combined pump-bearing performance was simulated hydraulically with the supply valve wide open and the bearings taking full pump discharge pressure. Approximate boiler flow and turbine thrust load were also simulated. Based on the data obtained during this test, it was concluded that the bearings would maintain the proper pump orientation, sufficiently low power loss, adequate lubricant flow, and load capacity within design specifications.

In addition to these tests, several nonpressurized starts were completed from zero to rated speed with the pump and bearings coupled together. Although scoring of the bearings resulted due to metallic contact between the turbine rotor and the housing caused by a fabrication error, it was concluded that a flooded unpressurized start is feasible.

7.3 System Test Packages

The first Snap I system package was an internally insulated Turbine Alternator Test Package (TATP) to evaluate turbine, alternator, and bearing performance, but did not include a pump. Modifications to the TATP package to incorporate the mercury pump resulted in the turbine-alternator-pump package (TAPP). Testing of the TAPP unit in the mercury vapor breadboard test facility established the operational ability of the bearings and other components in the TAPP package unit.

The externally insulated Prototype Test Package (PTP) was designed to incorporate the developed components, including the overhung jet-centrifugal mercury pump, the mercury lubricated hydrosphere bearings, a three-stage axial flow turbine, and a radial gap alternator. Preliminary testing of the PTP package unit was accomplished in the mercury vapor breadboard establishing operational ability and performance. Later system tests were conducted in the Systems Test Enclosure of the Snap I power conversion system, including the PTP package, boiler, condenser, and auxiliary equipment.

7.3.1 Turbine Alternator Test Packages (TATP)

The information obtained from these packages was beneficial to the bearings primarily as an indication as to the proper axial clearance to be pre-set at assembly and flow restriction sizes to be used in order to maintain adequate socket pressures and lubricant flow. This data was necessary to compensate for the thermal gradients encountered in the TATP package.

The major portion of the test work performed on the system was of a debugging nature during which time the related components and the auxiliary equipment were improved.

The hydrosphere bearings ultimately operated successfully throughout the range of speeds, loads, temperatures, and pressures encountered in these tests. The bearing data illustrated a satisfactory correlation with the performance obtained in the development testing discussed in Section 6.0.

7.3.2 Turbine-Alternator-Pump Package Tests (TAPP)

The major objective of the TAPP tests was to evaluate overall pump performance, its effect on bearing operation with the pump operating in a separate circuit, and to attempt coupling of the system pump discharge to the bearing supply, thus eliminating the auxiliary supply pump from the system.

Speed fluctuations caused by auxiliary equipment malfunctions resulted in large changes in pump and turbine thrust. The consequent transient loadings imposed on the bearings were in excess of design, but the bearings did not suffer any severe damage.

Coupling of the pump and bearings was performed with no impairment of performance in either component.

7.3.3 Prototype Test Package (PTP)

Experimental testing of the PTP package had the following bearing objectives:

1. To establish operational ability of the Snap I pump and bearings while coupled at design conditions.

2. To determine endurance capability of the hydrosphere bearings and the jet-centrifugal pump.

Adjustment of the pre-set, cold total axial bearing clearance was required to compensate for the different thermal gradients encountered in the PTP package due to the elimination of internal insulation.

The pump and bearings operated satisfactorily at design speed and pump inlet pressure on hot mercury for approximately 50 hours of continuous running. The total dynamic time while running on both nitrogen and mercury vapor driving fluid at various speeds and pump inlet pressures was approximately 67 hours. Since there was no decay in performance with time, this test gave the first positive indication the bearings of the prototype Snap 1 power conversion system could meet the endurance requirements.

7.3.4 Ground Test System (GTS)

The PTP unit was installed in the Systems Test Enclosure in conjunction with the boiler and condenser for final performance and endurance testing of the complete power conversion system.

During the course of the initial testing, the bearings were subjected to severe transient loadings, thermal gradients, and numerous starts and stops without serious damage being incurred.

After initial testing, including test rig and system modifications, the original PTP package was reworked and installed for endurance testing of the Snap 1 power conversion system. The system satisfactorily completed 2510 hours of continuous operation at design conditions and the bearings showed very stable operation, well within design requirements.

8.0 MATERIALS DEVELOPMENT

The requirements of the Snap I application impose several unique qualifications on the bearing materials:

a. The materials should be resistant to abrasion, scoring, and seizing.

b. The materials must not deteriorate in contact with mercury and must not contaminate mercury.

c. The materials must have thermal coefficients of expansion such that the radial clearance between the ball and socket be maintained so as not to affect bearing performance.

Blue Chip, a tungsten alloy high speed tool steel designated 18-4-1, was originally selected as the base material for both the ball and the socket. Several bearing materials and platings were evaluated in actual hydrosphere bearing operation during the experimental development program. Additional anti-scoring tests of a roller on a flat plate with liquid mercury as a lubricant were conducted by New Departure Division of General Motors to determine the relative anti-scoring qualities of ten promising materials pairs selected by TRW.

8.1 Experimental Hydrosphere Bearing Materials and Platings

The majority of the experimental development bearings consisted of 18-4-1 tungsten alloy Blue Chip high speed tool steel as a base material for both the ball and socket plus a plating on either or both components. Several bearing combinations of electrolized chrome plate, tungsten carbide flame plate, and blue chip tool steel components were tested. Flaking, cracking, and spalling of the platings resulted in premature abortion of these tests and eliminated platings from consideration as a final bearing surface. Other platings, surface treatments, and base materials were fabricated and some were tested and eliminated from further consideration.

After elimination of platings and surface treatments from considerations, successful hydrosphere bearing operation was obtained with a blue chip ball bearing component, subsystem, and system tests.

8.2 New Departure Anti-Scoring Tests

New Departure was given a subcontract to determine the anti-scoring characteristics of ten bearing material pairs. The purpose of the work was to obtain a qualitative, comparative ranking of the materials listed below for wear and scoring resistance in relationship with an 18-4-1 Blue Chip roller on an 18-4-1 flat plate. The tests consisted of rotating the one inch diameter roller (with a one inch spherical radius)

against a 1/2 inch x 1/2 inch x 1/4 inch flat for 30 minutes under a static load of one pound (40,000 spi compressive stress) and a surface speed of 5250 ± 150 fpm at 80°F and 500°F using liquid mercury as a lubricant.

Roller Specimen	Flat Specimen
18-4-1 Tool Steel	18-4-1 Tool Steel
CA-8 Tungsten Carbide	KL-150A Titanium Carbide
CA-8 Tungsten Carbide	Scottsonized 420 Stainless Steel
CA-8 Tungsten Carbide	Stellite Star J Cobalt Alloy
CA-8 Tungsten Carbide	Molybdenum
KL-150A Titanium Carbide	KL-150A Titanium Carbide
M-2 Tool Steel	KL-150A Titanium Carbide
Molybdenum	KL-150A Titanium Carbide
Molybdenum	9606 Pyroceram Ceramic
Molybdenum	Beryllium

Two of the most promising of the various mercury-lubricated bearing materials combinations, as determined by these frictional wear and bearing resistance tests, were submitted for metallurgical evaluation. These combinations consisted of an 18-4-1 tool steel roller rotating against an 18-4-1 flat which developed surface cracks, and a tungsten carbide roller rotating against a titanium carbide flat.

The diameter and depth of the worn impression in each flat was measured and is given in the table below:

		Worn Impression	
Material	Temperature	Diameter	Depth
18-4-1	80°F	0.079 inch	0.0010 inch
18-4-1	500°F	0.095	0.0021
Ti Carbide	80°F	0.035	0.000059
Ti Carbide	500°F	0.049	0.00047

These data show that the wear rate was greater at the higher temperature for each material tested.

Results of microscopic examination of the contacting roller and flat surface areas are summarized in Table 8-1. In general, the data show that the carbide combination is superior to the 18-4-1 tool steel combination with more damage occurring at the higher test temperature for each combination. The carbide flat appeared to suffer more damage than the carbide roller at each temperature, whereas the reverse condition was true for the 18-4-1 tool steel combination. Although the overall scoring and spalling damage appeared to be worse at 500°F than at 80°F for the 18-4-1 tool steel, the cracking appeared to be more severe in the 80°F test. The smooth, rounded pits which occurred in the titanium carbide flat tested at 500°F indicated either cavitation or corrosion damage or both.

TABLE 8-1

Results of Microscopic Examination of Contacting Surface Roller and Flat Area

Material	Temperature	Remarks
18-4-1 flat	80°F	Numerous cracks perpendicular to roller motion. Some scoring and dark streaks. See Figure 8-1.
18-4-1 roller	80°F	Numerous cracks transverse to roller motion. Spalled areas. See Figure 8-2.
18-4-1 flat	500°F	Some cracks similar to 80°F flat, however, not as numerous or as evident. More scoring and dark streaks than at 80°F.
18-4-1 roller	500°F	Some cracks similar to 80°F roller, however, not as numerous. More scoring and spalled areas than at 80°F.
Titanium Carbide flat	80°F	Some pits in cellular type structure. Practically no scoring.
Tungsten Carbide roller	80°F	Shiny, a few pits and no scoring.
Titanium Carbide flat	500°F	Extensive pits with rounded, fairly smooth walls in cellular type structure, inner-connected in direction of roller motion. Practically no scoring.
Tungsten Carbide roller	500°F	Some pitting with cellular type structure. Practically no scoring.

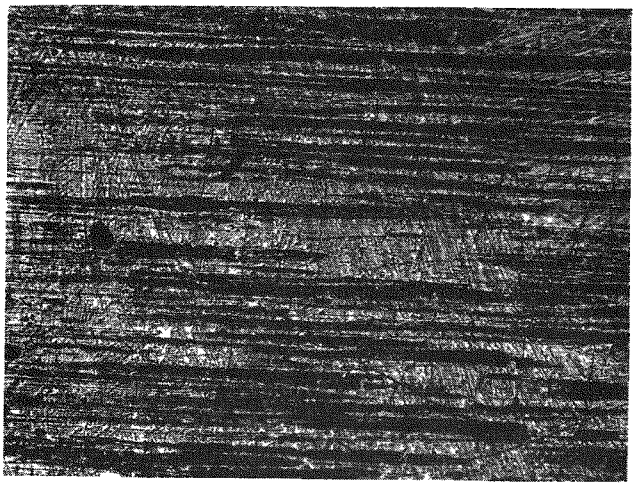

WEAR SURFACE OF 18-4-1 TOOL STEEL FLAT TESTED AT 80°F SHOWING SURFACE CRACKS PERPENDICULAR TO ROLLER MOTION 100X

FIGURE 8-1

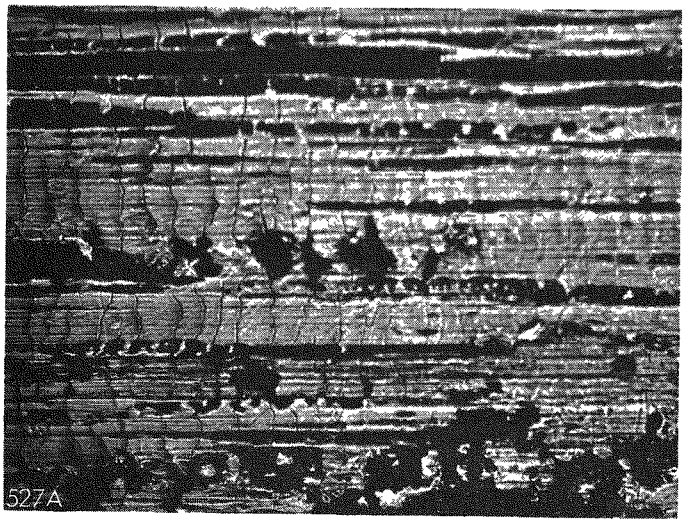

ROLLER SURFACE OF 18-4-1 TOOL STEEL TESTED AT 80°F SHOWING CRACKS PERPENDICULAR TO ROLLER MOTION AND FLAKED AREAS. 100X

FIGURE 8-2

Microscopic examination of the sectioned carbide rollers and flat (through the wear indentation) yielded no positive evidence of corrosion, metal transfer or pattern of wear, since the wear area was confined to the immediate surface where general surface irregularities made any observations insignificant. On the other hand, microscopic examination of the 18-4-1 tool steel specimens tested at both temperatures showed that the wear surface contained a soft, white layer ($KHN_{100g\ load}$ vs. KHN 1160 for base metal) with an adjacent zone heavily tempered. This indicated that excessively high temperatures were generated during testing. Also, cracks visible on the wear surface were found to extend inwards intergranularly about 0.0007 inches before changing direction parallel to the surface. Cracks below the surface running parallel to the surface were also noted. This type of cracking and the previously described pitting or flaking which occurred on the roller surfaces is characteristic of the surface fatigue of rolling surfaces due to repeated stressing under rotation.

The excessively high temperature generated during testing materially contributed to the fatigue failure of the 18-4-1 tool steel specimens, since this tool steel is adequate under light loading only to about 1100°F.

In conclusion, it may be stated that in order for the 18-4-1 tool steel to function as a satisfactory bearing material, the bearing temperature must be kept below 1000°F with adequate lubrication to prevent consequential bearing failure and the resultant deleterious bearing debris from entering the system.

Pictures of the test specimens are shown as Figure 8-3.

The conclusions based on the test results are listed below:

A. Of the ten material combinations tested at room temperature and at 500°F, greatest resistance to wear and scoring under the given test conditions was shown by a Tungsten Carbide roller rotating against a Titanium Carbide flat.
B. Three other material combinations were rated second, third and fourth in the order given without striking differences between their overall ratings:
    1. An 18-4-1 Blue Chip Tool Steel roller rotating against an 18-4-1 Tool Steel Flat.
    2. An M-2 Tool Steel roller against a Titanium Carbide flat.
    3. A Tungsten Carbide roller against a Cobalt Alloy flat.
C. Test results and material compatibility ratings are comparative ratings only, and the following factors should be taken into consideration:
    1. Carbide brittleness could lead to the fracturing of bearing components when operating in certain environments, such as those including mechanical or thermal shock.
    2. The surface cracking of 18-4-1 Tool Steel and Scottsonized 420 Stainless Steel could lead to detrimental effects, and thus warrant further study. This cracking could be characteristic of most steels.

ROLLER AND FLAT SPECIMEN MATERIALS RUN AT 500°F INITIAL OVEN AMBIENT TEMPERATURE

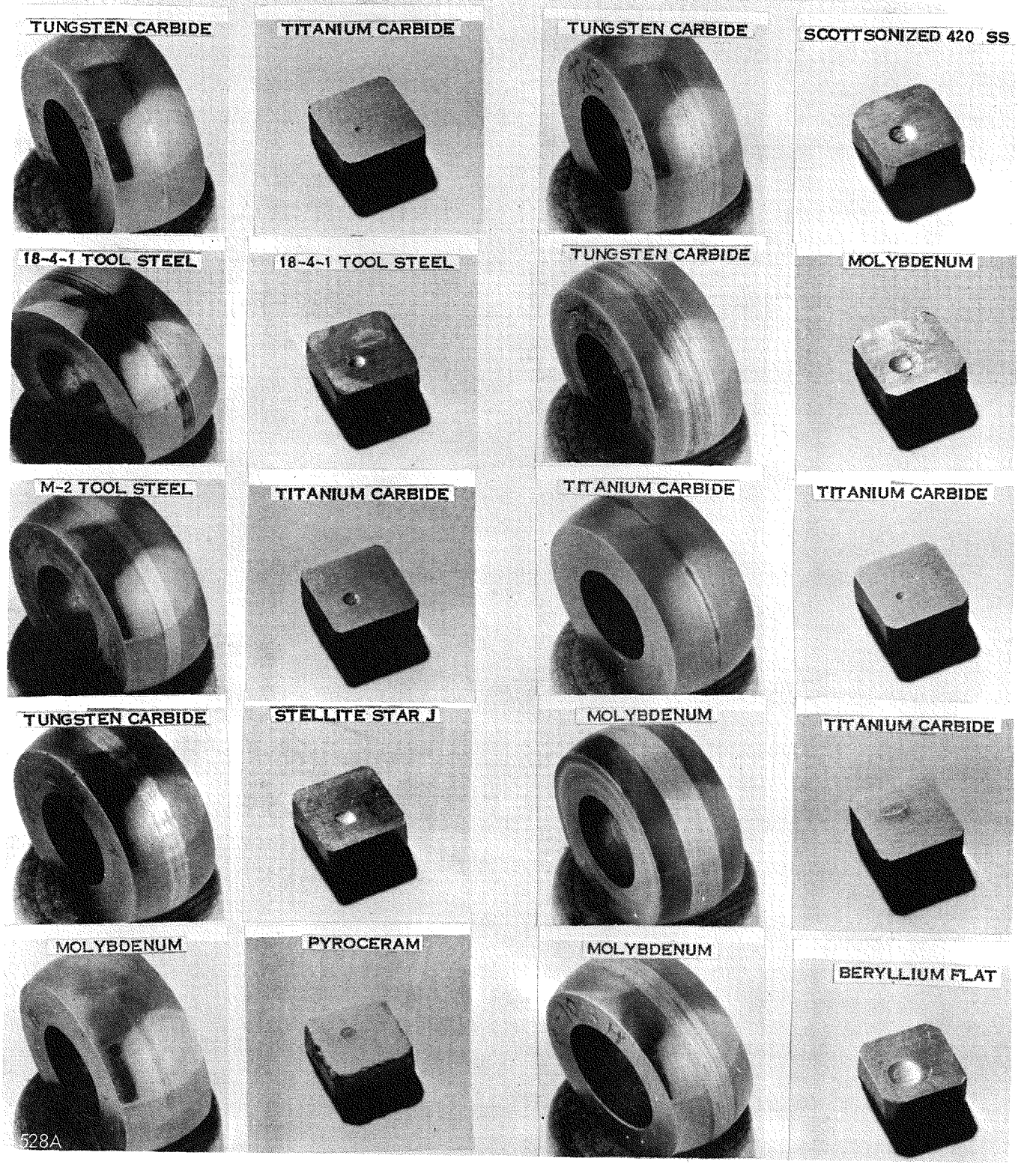

TEST CONDITIONS: LIQUID MERCURY LUBRICATION - ONE POUND LOAD

FIGURE 8-3

9.0 HYDROSPHERE BEARING FABRICATION, INSPECTION, AND ASSEMBLY

Specialized processes were developed for the fabrication, inspection, and assembly of the hydrosphere bearing due to its unique characteristics. The incorporation of the ball on the shaft prevented utilization of conventional machining techniques.

9.1 Hydrosphere Bearing Fabrication

Both the bearing and the socket were rough machined in the soft condition, heat treated, and then finish machined as follows:

1. The bearing socket was finish machined and lapped with a cast iron ball which has been machined to size (the bearing socket was measured by the diameter of the lapping ball).
2. The hydrosphere ball was machined and final lapped to the diameter which provides the desired initial radial clearance between the ball and socket. This diameter was checked with a dial indicator micrometer which was indexed with a master ball.

9.2 Hydrosphere Bearing Inspection Procedure

Before and after each test, the hydrosphere bearing and socket dimensions were recorded. A description of the method of obtaining the critical dimensions follows:

Socket - The socket diameter was measured within .0001 inch with cast iron lapping balls which have been machined to specific sizes. At the conclusion of the test, the same method was used to obtain the diameter with an accuracy of .0005". The loss in accuracy was due to irregularities of the surfaces caused by scoring and/or system contamination. A profile of the socket was made before and after each test on the "Indiron" recorder at distances of 1/16, 1/8 and 1/4 inches from the equator. A comparison of the profiles taken before and after the test provided a comparative profile from which wear or scoring patterns may be analyzed.

The socket was visually inspected under a x 45 power microscope for any surface imperfections, scratches, etc.

Ball - The hydrosphere bearing diameter was checked with a dial indicator micrometer which gave an accuracy of .0001". The ball was visually inspected under a x 45 power microscope for surface imperfections, scratches, etc.

Several metallographic analyses were made to determine if any intergranular action had occurred due to corrosion or erosion after the tests, and several attempts were made to obtain rechecks on diameters; however, the irregularities of the surfaces caused by scoring or system contamination made this impossible.

Ball and Socket Dual Bearing - The bearing diametral clearance at various total axial clearances was determined before and after each test. Both sockets were clamped in "V" blocks which were in turn clamped to a surface plate. The rotor assembly with the hydrospheres was floated between the two sockets with the balls bottomed in the sockets. One socket was moved away from the other socket .001 inch, resulting in the bearing assembly having a total axial clearance of .001 inch (equator of each ball and socket is .0005 inch apart in centered position). The shaft was bottomed in one of the sockets, and while the other was moved up and down, the total diametral movement was indicated on an electronic indicator. This procedure was repeated on the other bearing and at varying total axial clearance as desired.

10.0 BEARING TEST FACILITIES

10.1 Feasibility Bearing Test Rig

The original bearing test rig was basically a hydrosphere bearing feasibility rig. The capabilities of this rig were to rotate the bearing at 40,000 rpm and apply axial loads while measuring bearing torque. The mercury reservoir held a fixed amount of mercury whose flow rate to the bearings was a function of reservoir pressure and bearing clearance. The mercury, which could be heated to 500°F, was not recirculated, thereby limiting the duration of the test.

Due to the lack of instrumentation, the inability to apply radial loads, unavoidable misalignment, thermal expansion problems, and short term testing limitation, the test rig was redesigned and became known as the Modified Bearing Test Rig.

10.2 The Modified Bearing Test Rig

The modified bearing test rig was redesigned and is shown in Figure 10-1. The MBTR rig was used to obtain parametric data of various bearing configurations. The electrical drive motor was replaced by an air turbine to provide additional power, more accurate power measurements, and better speed control. The reservoir and feed line were redesigned to eliminate nitrogen leakage into the axial load pads. All of the pressure gauges which were attached to the test rig were replaced by pressure transducers to eliminate external loads on the bearings.

The rig was designed to have capabilities for:

a. Applying axial loads of 0-30 lbs and measuring them within ±3% accuracy.
b. Applying radial loads up to 20 lbs and measuring within ±1% accuracy.
c. The total power loss was determined with a torque transducer. However, due to the bearing slinger being partially immersed in mercury, the bearing power could only be estimated from past performance data.
d. The flow to the bearing was obtained by calibrating a capillary feed tube downstream of the pressurized reservoir. The accuracy of this measurement was 3%.
e. Bearing pressure distribution data was obtained from four pressure probes which are placed at 90° intervals radially around the bearing at 22 1/2° from the equator. These pressures were monitored by pressure transducers and an amplifier system with an estimated accuracy of ±3%.
f. The axial lift of the hydrosphere bearing was obtained from a capacitance transducer which is accurate to one microinch.
g. Radial displacement was obtained from four proximity transducers located at 90° intervals around the bearing shaft. These transducers were accurate to one microinch. However, instability of the test rig and the air piston resulted in misalignment of the hydrosphere and the socket and rendered the data quantitatively suspect.

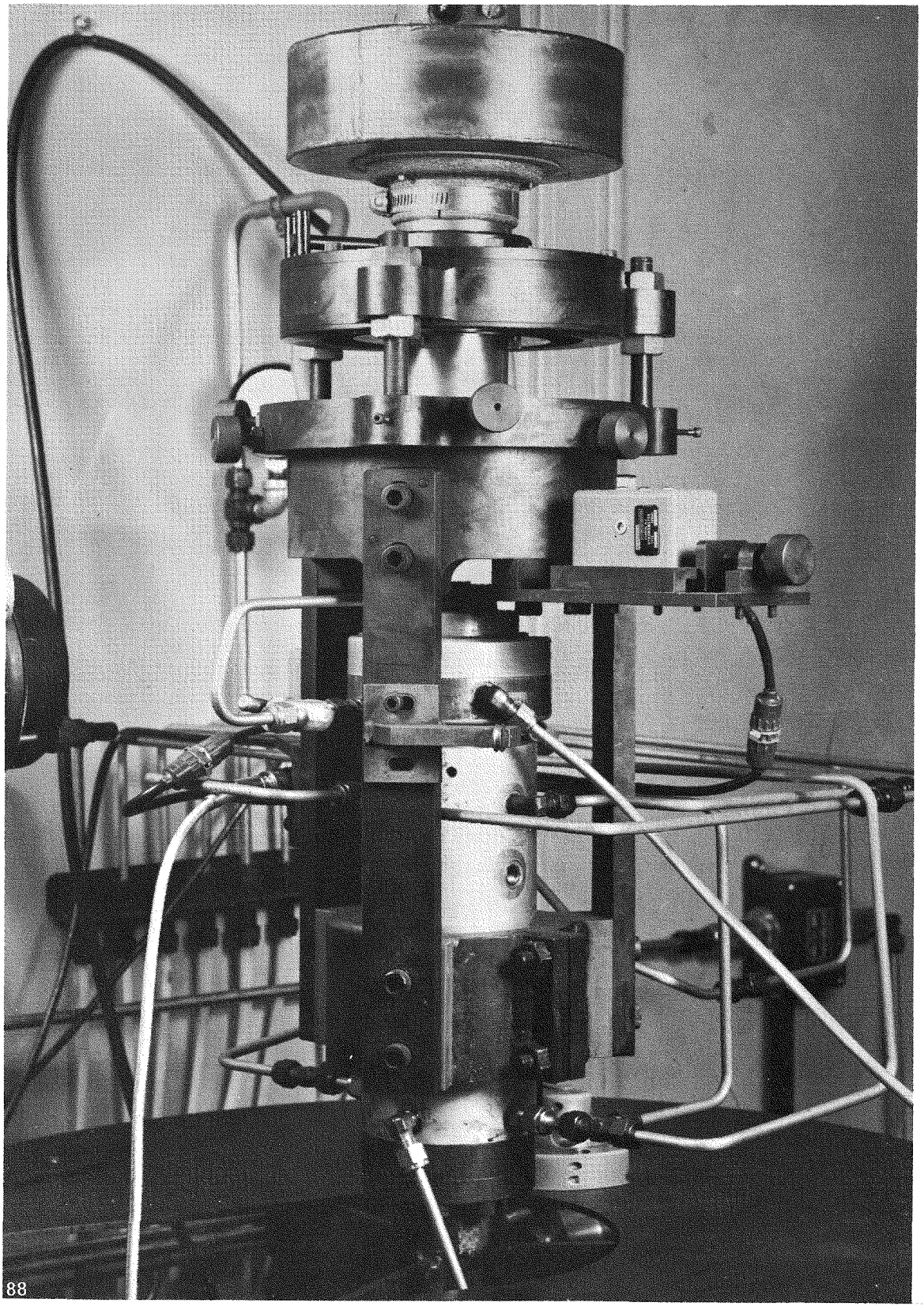

CLOSE UP VIEW - MODIFIED BEARING TEST RIG

FIGURE 10-1

h. The flow to the bearing is controlled by a fixed flow restriction located between the reservoir and the bearing. By proper sizing of the flow restriction the desired flow and bearing socket pressure can be obtained. Calibration of the fixed flow restriction can be utilized to obtain bearing flow to ±3%.

10.3 Free Running Bearing Test Rig

The free running bearing test rig was designed, as shown in Figure 10-2, to simulate the dual bearing construction of the final application. The rig incorporated flexibility in order that dual bearing (hydrospheres, or journals and thrust bearing) operation and the pump-bearing combination performance in a simulated package could be evaluated. Also provided were the plumbing and instrumentation necessary to calibrate the bearings of package units which were built up for the final application. The drive to rotate the bearings was a Terry-type turbine supplied with shop air. An air preheater was available to heat the turbine air. Incorporated in the test fixture were pressurized air load pads which applied various axial and radial loads simultaneously and/or individually to the bearings.

The bearing lubricant was supplied from a pressurized reservoir with N_2 cover gas. A Lapp Pulsafeeder proportioning pump which delivered 40 lbs/min liquid mercury at 300 psig supplied the reservoir. Facilities were incorporated into the test rig to enable the bearing supply, bearing socket, and pump discharge and back face pressures to be recorded with pressure transducers (range 0-400 psi) and a 6 channel brush recorder.

The externally applied axial load range of the rig was 0 to 60 lbs. This value does not include any axial loads that the associated components (such as pump impeller and air turbine) may have provided. The external load was applied on the turbine rotor end; thru air pads using shop air. Accuracy was 1/2%.

External radial loads to 50 lbs could be applied to the bearings in both the upward and downward directions. This did not include any radial loads exerted by the weight of the rotor, eccentricity of centerlines, etc. The external radial load was also applied to the bearing shaft by a pair of air pads using shop air with an accuracy of 1/2%. The possibility of the air loads acting as an air bearing at high speeds and reducing the actual load on the liquid-lubricated bearings was not fully evaluated.

Due to limitations of the pressure regulator, the maximum speed obtainable with 1/2 inch diameter bearings was 50,000 rpm. Speeds in excess of 60,000 rpm could probably have been obtained by preheating the air to the turbine or replacing the pressure regulator with a throttle valve with large flow passages.

Maximum available mercury supply to the test stand was 40 lbs/min @ 300 psi and 300° F. Pump-bearing operation with the pump and the bearings coupled was limited only by the pump output pressure and the measuring instruments available.

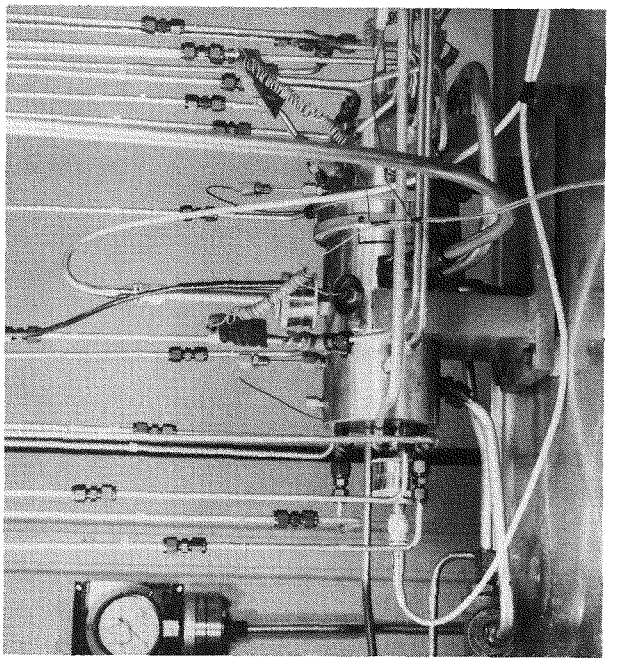

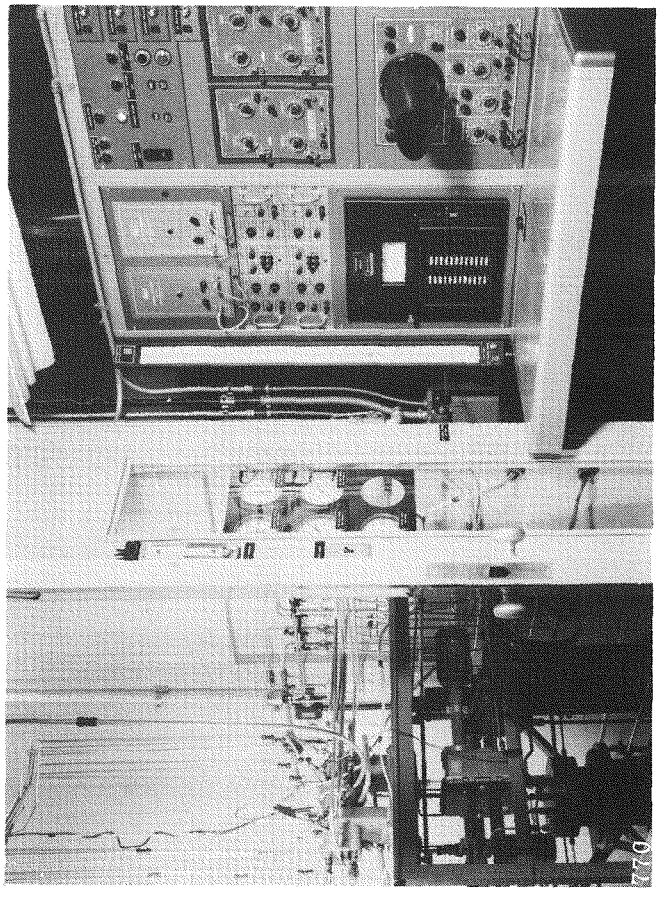

FREE RUNNING MERCURY BEARING TEST RIG

FIGURE 10-2

The test fixture was designed so that axial clearances up to .050 inch can be set with a pair of 1/2 inch diameter hydrospheres. Greater clearances could be obtained by decreasing the shaft length.

The bearing supply, bearing socket, pump discharge and backface pressures were measured by both gages and pressure transducers. Any sudden changes in the above pressures were recorded on a 6 channel Brush recorder. An audio-scope was available which, when attached to the test fixture, indicated possible scoring or malfunctions through changes in noise levels.

11.0 CONCLUSIONS AND RECOMMENDATIONS

The following conclusions were reached concerning hydrosphere design and performance.

1. Axial and radial loads of the magnitude encountered in the Snap I application can be sustained by the 1/2 inch hydrospheres.

2. Power losses as determined by more refined analysis and by test data are higher than originally predicted but are within the specification.

3. Dynamic stability of the lubricant film has been demonstrated consistently.

4. Flow rates are not excessive.

5. Small angular misalignment of the shaft can be tolerated without affecting performance.

6. The bearing is sensitive to small clearance changes which may arise from differential thermal expansion, from build-up of lubricant contaminant or from inadequate precision of fabrication. These effects, however, can be controlled.

7. Some hydrostatic support of radial loads has been demonstrated. This effect permits lifting the shaft prior to rotation.

8. Axial grooves in the socket tend to reduce radial load carrying capacity.

9. Contact stresses at nominal radial loads are high, but can be reduced to tolerable levels by proper design of the socket equator.

10. The best bearing materials for start-up and shut-down requirements, which have been wear tested to date, are tungsten carbide on titanium carbide. Mercury compatibility tests at 650°F for 1000 hours indicate some attack of the bonding matrix. However, for the lower temperatures anticipated in the bearing, compatibility and corrosion of the carbides do not appear to have a significant effect on bearing life. The 18-4-1 material, used in prototype tests, is also entirely satisfactory.

Further development work is necessary to:

1. Reduce power loss. The most promising method, which has not been fully investigated by test, appears to be a reduction in socket arc length in the axial direction. Direct power reduction, by means of reducing diameter, also appears possible.

2. Increase bearing tolerability to clearance reduction caused by contamination and

differential thermal expansion. From the bearing viewpoint, reduction in the production of contaminants by the system, a means for their exclusion from the bearings, and reduction of thermal gradients in the package would be desirable.

3. Increase flow restriction tolerability to flow area reduction as a result of contamination.

NOMENCLATURE

The following nomenclature and symbols are used in this report:

R = radius of socket, inches

c = radial clearance, inches

c' = c/R, clearance ratio

θ = angle from axis of rotation to radius at film thickness, degrees

h = film thickness, inches

ℓ = axial displacement of ball center, inches

ℓ' = ℓ/R, lift ratio

R_o = inlet radius, inches

θ_o = inlet angle, degrees

C = flow constant

$\dot{w}$ = flow, pounds/minute

W_T = thrust capacity, pounds

H = frictional power, watts

μ = absolute viscosity, lb sec^2/in^2

ρ = mass density, lb sec^2/in^4

ν = kinematic viscosity, in^2/sec

K_P = film pressure factor

K_Q = flow factor

p = film pressure, psig

p_o = socket inlet pressure, psig

NOMENCLATURE (Continued)

T = frictional bearing torque, inch pounds

I = moment of inertia of shaft, lb sec^2/in

α = angular deceleration, rad/sec^2

K_w = windage constant

p_m = socket discharge pressure, psig

The following refer only to Figure 4-1.

x, y, z = coordinate directions

$\bar{u}, \bar{u}, w$ = mean streamline velocity

U = sliding surface velocity

s = distance slong mean streamline

N = normal distance along mean structure

ω = shaft speed

α = angle between tangent to mean streamline and meridian of spherical socket.

BIBLIOGRAPHY

The reports listed in the bibliography are not available for general distribution. Any inquiries concerning the availability of this information should be directed to the AEC.

EN 452	Operational Characteristics of Jet Centrifugal Pump Hydrosphere Bearing Combination in FRR	2/11/59	Secret
EN 581	Performance of S/N 23 and 25 Pump Bearing Combination	5/29/59	Secret
EN 600	PTP I Pump and Bearing Performance	6/8/59	Secret
TM 1353	Summary of Bearing Performance and System Tests	2/12/59	Secret
ER 3096	Bearing and Journal Materials Compatible with Mercury as Lubricating Medium	10/8/56	-

REFERENCES

1. Shaw, M.C. and Macks, E.F., Analysis of Lubrication of Bearings McGraw-Hill, 1949.

2. Shaw, M.C. and Strang, C.D., The Hydrosphere - A New Hydrodynamic Bearing, ASME Journal of Applied Mechanics, June 1948.

3. Goodzeit, C.L., Compatibility of Metals in Bearing Contact, ASME Transactions 58MD9, April 1958.